Divergence of TORC1-mediated Stress Response Leads to Novel Acquired Stress Resistance in a Pathogenic Yeast

Jinye Liang[^1], Hanxi Tang[1#], Lindsey F. Snyder[2#], Christopher E. Youngstrom[1], Bin Z. He[^1]

[1]Biology Department, The University of Iowa, Iowa City, IA 52242
[2]Interdisciplinary Graduate Program in Genetics, The University of Iowa, Iowa City, IA 52242

[#]These authors contributed to the work equally
[^]Correspondence should be addressed to
Bin Z. He, bin-he@uiowa.edu
Jinye Liang, jinye-liang@uiowa.edu

Running title: Evolution of acquired stress resistance for H_2O_2 in yeasts

Keywords: acquired stress resistance, gene regulatory evolution, phosphate starvation, oxidative stress, opportunistic yeast pathogen, TORC1, stress response

Abstract

Acquired stress resistance (ASR) enables organisms to prepare for environmental changes that occur after an initial stressor. However, the genetic basis for ASR and how the underlying network evolved remain poorly understood. In this study, we discovered that a short phosphate starvation induces oxidative stress response (OSR) genes in the pathogenic yeast *C. glabrata* and protects it against a severe H_2O_2 stress; the same treatment, however, provides little benefit in the low pathogenic-potential relative, *S. cerevisiae*. This ASR involves the same transcription factors (TFs) as the OSR, but with different combinatorial logics. We show that Target-of-Rapamycin Complex 1 (TORC1) is differentially inhibited by phosphate starvation in the two species and contributes to the ASR via its proximal effector, Sch9. Therefore, evolution of the phosphate starvation-induced ASR involves the rewiring of TORC1's response to phosphate limitation and the repurposing of TF-target gene networks for the OSR using new regulatory logics.

Introduction

Acquired stress resistance (ASR) is the phenomenon where organisms exposed to a non-lethal primary stress become more resistant to a secondary severe stress of the same or a different type (Lu *et al.* 1993; Leroi *et al.* 1994; Lou and Yousef 1997; Durrant and Dong 2004; Scholz *et al.* 2005; Hecker *et al.* 2007). Widely observed across kingdoms of life, ASR is believed to provide a survival advantage in environments with predictable changes. For example, it was shown in *S. cerevisiae* that stressors occurring early during fermentation, e.g., heat and ethanol, have a strong protective effect against stresses that occur later, such as oxidative stress, while the reverse is not true (Mitchell *et al.* 2009). This asymmetry in cross-stress protection suggests that ASR is not simply a general stress response but rather represents an adaptive anticipatory response, enabling cells to predict and survive future challenges. A natural prediction is that ASR must be adapted to the specific stress patterns organisms encounter in their environments, leading to divergence between species.

Despite the potential role of ASR in adaptation, we know little about its evolution. ASR is known to have biochemical, post-translational or transcriptional mechanisms (Davies 2016; Goulev *et al.* 2017). At the transcriptional level, studies in *S. cerevisiae* showed that ASR does not rely on a single, all-purpose program; instead, genes involved in ASR are regulated in a stress-specific manner (Gasch *et al.* 2000). Furthermore, ASR against the same secondary stress is dependent on distinct genes that are regulated by different types of primary stresses (Berry *et al.* 2011). Such stress-specific regulation enables mutations to target specific contexts and avoid pleiotropic effects, thereby facilitating the evolution of ASR. However, few studies dissected ASR in closely related species. Previous studies on ASR in yeasts, for example, have primarily focused on comparing *S. cerevisiae* with distantly related species, such as *C. albicans* and *S. pombe*, which are estimated to have diverged from the baker's yeast ~200 and ~500 million years ago (Chen *et al.* 2003; Rodaki *et al.* 2009; Rhind *et al.* 2011; Shen *et al.* 2018; Brown *et al.* 2020). These substantial evolutionary distances, coupled with the whole genome duplication (WGD) event specific to *S. cerevisiae*, significantly hindered our ability to discern the evolutionary alterations behind ASR divergence.

In this study, we focused on the more closely related *S. cerevisiae* and *C. glabrata*, both of which are post-WGD and share more than 90% of their genes with one-to-one orthologs (Dujon *et al.* 2004). Even though *C. glabrata* is evolutionarily close to *S. cerevisiae*, it is distinguished by its ability to colonize and infect humans (Kumar *et al.* 2019; Zakhem *et al.* 2021). As one of the most frequent causes for Candidiasis, it shares many phenotypic traits with the distantly related pathogen, *C. albicans*, including high resistance to host-associated stresses such as the oxidative stress (Fidel *et al.* 1999; Brunke and Hube 2013). In fact, it exhibits the highest resistance to H_2O_2 in a broad phylogenetic survey of fungi (Nikolaou *et al.* 2009). Apart from oxidative stress, host immune systems also use other stressors, such as nutrient limitation, to kill invading microbes (Seider *et al.* 2014). Given the array of challenges they encounter, it is probable that yeast pathogens such as *C. glabrata* evolved anticipatory responses to help them prepare for impending stresses (Brown *et al.* 2020). Interestingly, we and others found that *C. glabrata, C. albicans* and a more distantly related pathogen, *Cryptococcus neoformans*, all have an expanded phosphate starvation (PHO) response compared with that in *S. cerevisiae*,

including the induction of oxidative stress response (OSR) genes (Ikeh *et al.* 2016; He *et al.* 2017; Lev *et al.* 2017). As an essential macronutrient, fungal cells must acquire phosphate from the environment. Emerging evidence suggests that responses to phosphate limitation play a crucial role in the host-fungal interaction. First, a defective PHO pathway, either by deleting the transcription factor (TF) *PHO4* or the high affinity phosphate transporter *PHO84*, leads to reduced virulence and survival for *C. albicans* inside macrophages and animal models (Ikeh *et al.* 2016, 2017; Liu *et al.* 2017, 2018). Second, two clinical isolates of *C. albicans* exhibit enhanced virulence in a phosphate-dependent manner in both a *C. elegans* and a mouse model of infection (Romanowski *et al.* 2012). Third, several PHO genes were found to be upregulated in phagocytosed *C. glabrata* cells, suggesting that yeast cells experience phosphate limitation inside the phagosome (Rai *et al.* 2021).

We found in this study that a short-term phosphate starvation led to the induction of at least 15 OSR genes and enhanced the survival of *C. glabrata* against a severe H_2O_2 stress. The same treatment had little to no effect in the related *S. cerevisiae*. Using transcriptional profiling, genetic perturbations, reporter and survival assays, we identified key players in the network underlying the ASR, including the catalase gene *CTA1*, transcription factors (TFs) Msn4 and Skn7 and homolog of the Greatwall kinase, Rim15. We found that phosphate limitation quickly and strongly suppressed the Target-of-Rapamycin Complex 1 (TORC1) in *C. glabrata* but not in *S. cerevisiae*; the proximal effector Sch9 was also shown to contribute to the ASR in the former species, strongly implicating TORC1 as a major contributor to the divergence in ASR. In summary, our results identified a key signaling-TF-effector gene subnetwork underlying the divergent ASR phenotype and thereby provides a concrete example of ASR evolution.

Results

Phosphate starvation provides strong acquired resistance for H_2O_2 in *C. glabrata* but not in *S. cerevisiae*

Based on the evidence linking phosphate to oxidative stress and virulence in *C. glabrata* and *C. albicans*, we asked whether phosphate starvation could provide acquired resistance for severe H_2O_2 stress in *C. glabrata* and whether the behavior is different in the low pathogenic-potential relative, *S. cerevisiae*. To answer this question, wild type cells from both species were subjected to 45 minutes of phosphate starvation, followed by a severe H_2O_2 challenge (Fig. 1A). We designed the experiment to be able to compare the ASR effect between species despite differences in their basal resistance level to H_2O_2, which affects the magnitude of ASR (Berry and Gasch 2008). Through titration, we found that 100 mM and 10mM H_2O_2 resulted in a similar ~2.5% survival in *C. glabrata* and *S. cerevisiae*, respectively (Fig. S1A, P = 1, Materials and Methods). Using these concentrations as the secondary stress, we found that phosphate starvation greatly enhanced the survival of *C. glabrata* after the H_2O_2 stress (Fig. 1B) but had no detectable effect in *S. cerevisiae* (Fig. 1C). A quantitative colony forming unit (CFU) assay confirmed this (Fig. 1D, raw P = 0.0039 and 0.37 in *C. glabrata* and *S. cerevisiae*, respectively). To quantify the magnitude of ASR, we defined ASR-score as the fold increase in survival due to the primary stress treatment, i.e., the ratio between the survival rates with (r') and without (r) the primary stress. Using this definition, we found a 45-minute phosphate starvation led to an ASR-

114 score of 3.4 in *C. glabrata* (95% CI: [2.66, 4.26]), compared with 1.3 in *S. cerevisiae* (95% CI:
115 [0.90, 1.63]). To comprehensively test the relationship between phosphate starvation and ASR
116 for oxidative stress, we altered both the severity of the secondary stress and the length of the
117 primary stress and asked how this affected ASR in both species. We found that more severe
118 secondary stress (higher [H_2O_2]) led to stronger ASR in *C. glabrata* but not in *S. cerevisiae* at
119 the concentrations tested (Fig. S1B). When we increased the primary phosphate starvation
120 treatment to 90 and 135 minutes, we observed a stronger ASR in *C. glabrata* (ASR-scores =
121 111 and 170, $P < 0.05$ after Bonferroni correction, Fig. S1C). A similar trend was observed in *S.*
122 *cerevisiae* (ASR-score = 11 and 22) but didn't reach statistical significance (Bonferroni-
123 corrected $P = 0.7$ and 0.5).

124 We also wondered whether the ASR for H_2O_2 is systematically different between the two
125 species or whether phosphate starvation represents a distinct case of divergence. To answer
126 this question, we tested two other stresses, heat shock and glucose starvation, and found that
127 both led to ASR at a similar level between the two species (Fig. S2). Therefore, we conclude
128 that *C. glabrata* and *S. cerevisiae* diverged particularly in the phosphate starvation-induced ASR
129 for H_2O_2, where *C. glabrata* showed a strong ASR while the same primary stress elicited a much
130 weaker effect in *S. cerevisiae*.

131 Lastly, we asked if phosphate starvation provides protection for other oxidative stress
132 agents by replacing the secondary stress with either tert-butyl hydroperoxide (tBOOH), an alkyl
133 hydroperoxide, or menadione (menadione sodium bisulfite, MSB), a superoxide agent. We
134 found that phosphate starvation does not provide ASR for tBOOH, while a moderate ASR effect
135 was observed for menadione compared to H_2O_2 (Fig. S3). We conclude that the existence and
136 magnitude of phosphate starvation-induced ASR depends on the nature of the ROS. This result
137 supports the prediction that ASR is specific to the primary and secondary stress combinations
138 rather than being a general cross-stress protection mechanism (Mitchell *et al.* 2009).

139 **Oxidative stress response genes were induced under phosphate starvation in *C. glabrata***

140 One potential mechanism for the observed ASR in *C. glabrata* is that phosphate starvation led
141 to the induction of oxidative stress response (OSR) genes during the primary stress (Fig. 2A).
142 To test this, we curated a set of H_2O_2-response genes in the well-studied *S. cerevisiae*, which
143 include antioxidants, proteases, chaperones and other genes to scavenge ROS and mitigate
144 ROS-induced damages, as well as the TFs regulating them (Lee *et al.* 1999; Hasan *et al.* 2002).
145 Using this reference set (Table S1), we identified their orthologs in *C. glabrata* and asked if they
146 were induced during phosphate starvation. To do so, we profiled the transcriptional response at
147 1 hour of phosphate starvation in *C. glabrata* and compared it with the response to the same
148 treatment in *S. cerevisiae* from (Zhou and O'Shea 2011). Of the 29 genes tested, 15 were
149 significantly induced by at least two-fold in *C. glabrata* (FDR < 0.05), compared with three in *S.*
150 *cerevisiae* (Fig. 2B-F). These include antioxidant genes such as *CTA1*, *PRX1*, *SOD1* and
151 *SOD2*. Induction of these OSR genes could lead to enhanced ROS scavenging and protection
152 against oxidative damages in *C. glabrata*, consistent with its stronger ASR effect (Jamieson
153 1998; Mason *et al.* 2005; Welker *et al.* 2010; Reichmann *et al.* 2018).

154 ***CTA1* is required for the ASR for H_2O_2 but not during phosphate starvation in *C. glabrata***

155 To test the hypothesis that the induction of OSR genes contributed to the ASR, we focused on
156 *CTA1*, which has a well-established role in the resistance to H_2O_2 in *C. glabrata* (Cuéllar-Cruz *et*
157 *al.* 2008). We first used qRT-PCR to confirm that *CTA1* is ~3 fold induced after 45 minutes of
158 phosphate starvation (Fig. 3A). We also confirmed that Cta1 protein levels increased during
159 phosphate starvation by endogenously tagging Cta1 with GFP (Fig. 3B). Notably, this strain had
160 the same H_2O_2 resistance as the wild type (Fig. S4A). To determine if *CTA1* is required for the
161 phosphate starvation-induced ASR in *C. glabrata*, we created a *cta1*Δ strain and compared its
162 ASR phenotype to the wild type using comparable strengths of H_2O_2. We found that loss of *cta1*
163 largely abolished the phosphate starvation-induced ASR for H_2O_2 (Fig. 3C). Quantitative CFU
164 assays revealed a residual ASR effect in *cta1*Δ (ASR-score = 1.5, 95% CI [1.2, 1.8]), which was
165 significantly lower than that in the wild type strain (ASR-score = 9.8, 95% CI [5.5, 15], Mann-
166 Whitney's U test comparing the two genotypes, $P = 0.001$) (Fig. 3D). The ASR defect in *cta1*Δ
167 was rescued by putting *CTA1* back into its endogenous locus (Fig. S4B, C). To determine if
168 *CTA1* induction is sufficient to confer ASR, we replaced the endogenous promoter of *CTA1* with
169 an inducible *MET3* promoter. We confirmed that *MET3pr-CTA1* was induced to a comparable
170 level in the induction media as the endogenous *CTA1* under phosphate starvation at 45 min
171 (Fig. S5A). Using this strain, we found that pre-inducing *CTA1* enhanced the survival of the cells
172 during the secondary stress as did phosphate starvation (Fig. S5B, C). We therefore conclude
173 that *CTA1* induction is both necessary and sufficient for the ASR. It's worth noting this doesn't
174 rule out the contribution of other OSR genes induced under phosphate starvation (Fig. 2).
175 One question that remained was whether the induction of *CTA1* and other OSR genes
176 served strictly to enhance the survival during the secondary stress, or if they were part of the
177 primary stress response, with an unintended benefit for the secondary stress. To distinguish
178 between these two hypotheses, we asked if Cta1, or the main TF for the canonical OSR, Yap1,
179 were required for survival under phosphate starvation. We found that deletion of neither gene
180 affected growth relative to the wild type during phosphate limiting conditions, while a strain
181 deficient in the PHO response showed severe growth defects (Fig. S6A). We conclude that the
182 induction of *CTA1* primarily serves the secondary H_2O_2 stress. Lastly, we found that while *CTA1*
183 is crucial for the phosphate starvation-induced ASR for H_2O_2, it is less important with mild H_2O_2
184 used as the primary stress (Fig. S6B). This result supports the previous finding that the genetic
185 basis for ASR is highly variable and dependent on the primary stress (Berry *et al.* 2011).

186 **Msn4 and Skn7 contribute to *CTA1* induction during phosphate starvation in *C. glabrata***

187 We reasoned that TFs involved in *CTA1* induction during phosphate starvation must be key to
188 the ASR. Four TFs were implicated in *CTA1*'s induction in *C. glabrata* under H_2O_2 stress, i.e.,
189 Yap1, Skn7, Msn2 and Msn4 (Cuéllar-Cruz *et al.* 2008). To determine which one(s) contributes
190 to *CTA1* induction under phosphate starvation, we deleted each TF and measured Cta1-GFP
191 induction. We found that *yap1*Δ and *msn2*Δ didn't affect Cta1 induction, while *msn4*Δ and *skn7*Δ
192 both exhibited decreased Cta1 induction during phosphate starvation (Fig. 4A). A double mutant
193 *msn4*Δ *skn7*Δ exhibited a stronger reduction in Cta1-GFP than either TFΔ alone, suggesting that
194 both Msn4 and Skn7 were required for *CTA1* induction (Fig. 4A). However, since Cta1-GFP was
195 still induced in the *msn4*Δ *skn7*Δ strain, additional TFs must be involved.

196 We also measured Cta1 induction during H_2O_2 treatment and confirmed that both Yap1
197 and Skn7 were required, while *msn4*Δ resulted in a slight decrease in induction and *msn2*Δ had
198 no measurable effect under the H_2O_2 concentration tested (Fig. S7). This showed that the
199 induction of the same effector gene, *CTA1*, depended on different TF combinations under
200 different stresses, a result consistent with previous findings in *S. cerevisiae* (Gasch *et al.* 2000).
201 To determine if Msn4 and Skn7 directly regulate *CTA1* under phosphate starvation, we
202 first predicted their binding sites in the promoter of *CTA1* (Fig. 4B). This allowed us to construct
203 a series of promoter mutants, including two internal deletions (200 bp) removing the predicted
204 Msn4 or Skn7 binding sites, as well as point mutations predicted to abrogate Msn4 and Skn7
205 binding (Fig. 4B). For both TFs, we found that all promoter mutants exhibited reduced Cta1-GFP
206 levels similar to the TF deletion strain, with the 200 bp deletion mutants showing the most
207 severe phenotypes (Fig. 4C, D). These results strongly suggest that Msn4 and Skn7 directly
208 regulate *CTA1* during phosphate starvation. In summary, we found that Msn4 and Skn7, along
209 with unidentified TFs, jointly regulate *CTA1* induction in *C. glabrata* under phosphate starvation,
210 while Yap1 and Skn7 were the main TFs responsible for its induction under H_2O_2 stress.

211 **Msn4 translocates into the nucleus upon phosphate starvation in *C. glabrata***

212 The activity of Msn4 and its paralog Msn2 are partially regulated via nuclear translocation in
213 both *C. glabrata* and *S. cerevisiae* (Görner *et al.* 1998; Cuéllar-Cruz *et al.* 2008; Roetzer *et al.*
214 2008; Boisnard *et al.* 2009). We therefore asked if Msn4 orthologs respond differently to
215 phosphate starvation in *C. glabrata* vs *S. cerevisiae*. Using GFP-tagged Msn4 and fluorescent
216 microscopy, we found that phosphate starvation led to 47% of the *C. glabrata* cells to have
217 nuclear localized Msn4 ($Msn4^{nuc}$), compared with < 4% in *S. cerevisiae* (Fig. 5, Bonferroni
218 corrected $P < 0.01$). This divergence is condition-specific: glucose starvation led to a similar
219 level of $Msn4^{nuc}$ in both species (Fig. 5, 76% in *C. glabrata* vs 73% in *S. cerevisiae*, raw $P =$
220 0.7). No significant difference was observed between species under the no-stress condition (raw
221 $P = 1$). These results further support CgMsn4 as one of the TFs mediating the phosphate
222 starvation induced ASR in *C. glabrata* and that divergence in how Msn4 responds to phosphate
223 starvation is a major contributor to the species divergence in ASR. In contrast, we found that the
224 paralog Msn2 translocated into the nucleus in a comparable fraction of cells in the two species
225 under phosphate starvation: 52% in *C. glabrata* and 54% in *S. cerevisiae* (Fig. S8, $P = 0.8$).
226 Combined with the lack of effect of *msn2*Δ on Cta1 induction, we conclude that Msn2 is not
227 involved in the ASR and doesn't contribute to its divergence.

228 **The Greatwall kinase, Rim15, is an important signaling component in the ASR network**

229 Given Msn4's role in the phosphate starvation-induced ASR in *C. glabrata* (Fig. 4, 5), we used it
230 as a bait to identify upstream signaling components in the ASR network. In *S. cerevisiae*, a key
231 regulator of Msn2/Msn4 activity is the Greatwall kinase, Rim15 (Lee *et al.* 2013; Plank 2022).
232 Rim15 itself is regulated by multiple nutrient and stress-sensing kinases, e.g., TORC1, PKA and
233 Pho80/85, making it a hub for integrating nutrient and stress signals (Pedruzzi *et al.* 2003;
234 Swinnen *et al.* 2006). We hypothesize that Rim15 regulates the nuclear localization of Msn4
235 during the primary stress in *C. glabrata* (Fig. 6A). To test this, we compared the nuclear
236 localization of CgMsn4-GFP in the wild type and *rim15*Δ backgrounds. We found that ~68% of
237 the wild type cells had nuclear-localized CgMsn4 during phosphate starvation, compared with

238 only 22% in the *rim15*Δ background (Fig. 6B, $P < 0.001$). By contrast, both strain backgrounds
239 showed a low fraction of cells with CgMsn4^{nuc} under high phosphate conditions (Fig. 6B, $P =$
240 0.2). Next, we asked if Rim15 is required for *CTA1* induction. We found that *rim15*Δ reduced
241 Cta1-GFP induction to a similar level as *msn4*Δ, supporting its role as a regulator of the ASR
242 (Fig. 6C). *msn4*Δ *rim15*Δ had a more severe effect than either deletion alone, suggesting
243 additional players besides the Rim15-Msn4 pathway (Fig. 6C). Lastly, to assess the role of
244 Rim15 in the phosphate starvation-induced ASR, we performed quantitative CFU assays to
245 compare the wild type and *rim15*Δ strains at a comparable strength of H_2O_2 (Fig. 6D). While
246 there is a significant ASR effect in both strains (both raw $P = 0.008$), the ASR effect is weaker in
247 *rim15*Δ cells (mean ASR-score = 3.45 for *rim15*Δ, 95% CI = [2.54, 4.33]; mean ASR-score =
248 6.29 for the WT, 95% CI = [4.58, 8.53], Mann-Whitney U test between genotypes, two-sided $P =$
249 0.04). This ASR defect was rescued by putting *RIM15* back to its endogenous locus (Fig. S9).
250 Taken together, these results strongly suggest that Rim15 is a crucial signaling component for
251 the phosphate starvation-induced ASR in *C. glabrata*.

252 **Target-Of-Rapamycin Complex 1 (TORC1) is strongly inhibited by phosphate starvation**
253 **in *C. glabrata* but not in *S. cerevisiae***

254 In *S. cerevisiae*, Msn2 and Msn4's nuclear translocation is regulated by both the Target-of-
255 Rapamycin Complex 1 (TORC1) and Protein Kinase A (PKA) pathways (Görner *et al.* 1998;
256 Beck and Hall 1999; Plank 2022). In *S. cerevisiae*, TORC1 responds slowly and weakly to
257 phosphate limitation (Urban *et al.* 2007). In the distantly related yeast pathogen *C. albicans*,
258 TORC1 was shown to respond rapidly to phosphate availability (Liu *et al.* 2017). We therefore
259 hypothesized that TORC1 is more strongly and quickly inhibited by phosphate starvation in *C.*
260 *glabrata* than in *S. cerevisiae*, contributing to the Msn4-mediated stress response and ASR. To
261 test this, we used the phosphorylation of ribosomal protein S6 (Rps6) as a conserved readout of
262 TORC1 activity (Magnuson *et al.* 2012; González *et al.* 2015; Liu *et al.* 2017). We found that 60
263 minutes of phosphate starvation did not affect the total level of Rps6 but markedly reduced the
264 abundance of phosphorylated Rps6 (P-Rps6) in *C. glabrata* (Bonferroni-corrected $P = 0.06$, Fig.
265 7A, B). The same treatment, however, did not affect the proportion of P-Rps6 in *S. cerevisiae* (P
266 $= 1$). By contrast, nitrogen starvation rapidly inhibited phosphorylation of Rps6 in both species
267 ($P = 0.06$ and 0.07). These results confirmed that inhibition of TORC1 by nitrogen starvation is
268 conserved between the two species while only in *C. glabrata* is TORC1 strongly inhibited by
269 phosphate starvation at 60 minutes, consistent with their distinct ASR phenotypes (Fig. 1). To
270 determine which of the two species represents the ancestral state, we performed the same P-
271 Rps6 assay in two outgroup species, *K. lactis* and *L. walti*, which diverged from *S. cerevisiae*
272 and *C. glabrata* approximately 120 million years ago (Shen *et al.* 2018). Both species exhibited
273 intermediate levels of TORC1 inhibition by phosphate starvation at 60 minutes, suggesting that
274 phosphate signaling to TORC1 is ancestral, but the signaling strength has evolved (Fig. S10).
275 By contrast, in all four species TORC1 was rapidly inhibited by nitrogen starvation, suggesting
276 that nitrogen is an evolutionarily conserved input for TORC1.

277 **Inhibition of TORC1 leads to Msn4 nuclear localization, *CTA1* induction and confers mild**
278 **ASR in *C. glabrata***

279 To determine if TORC1 inhibition can lead to ASR, we used rapamycin to specifically inhibit
280 TORC1 and monitored Msn4^{nuc}, Cta1-GFP induction and the ASR effect. We found that
281 TORC1-inhibition induces Msn4^{nuc} in both species, with a stronger effect in *C. glabrata*: 45 min
282 of exposure to 500 ng/mL of rapamycin causes 71.8% (79/110) of *C. glabrata* cells and 14.5%
283 (19/131) of *S. cerevisiae* cells to have Msn4^{nuc}. Both were significantly higher compared with the
284 mock-treated group (1.8% in *C. glabrata* and 1.2% in *S. cerevisiae*, raw FET $P < 0.001$ in both).
285 Next, we followed Cta1-GFP induction in *C. glabrata* exposed to rapamycin and found a dose-
286 dependent response except for the highest dose, which resulted in a lower induction than the
287 next dose (Fig. 7C). Lastly, we found 125 ng/mL rapamycin treatment for 45 minutes modestly
288 but significantly enhanced the survival of *C. glabrata* following a secondary H_2O_2 stress (Fig.
289 7D, mean ASR-score = 1.79, 95% CI [1.35, 2.28], raw $P = 0.016$). The same rapamycin dose
290 resulted in a similar increase in survival in *S. cerevisiae* (mean ASR-score = 1.81, 95% CI [1.21,
291 2.47], raw $P = 0.063$) (Fig. 7E). We conclude that TORC1 inhibition has the potential to induce
292 acquired resistance for H_2O_2 in both species. This implies that divergence of the ASR occurred
293 through TORC1's differential response to -Pi.

294 **TORC1 proximal effector, Sch9, contributes to phosphate starvation-induced ASR, while**
295 **a downstream output of the Tap42-PP2A branch is minimally affected**

296 The AGC kinase Sch9 is directly phosphorylated and regulated by TORC1 (Urban *et al.* 2007).
297 In turn, Sch9 regulates multiple downstream processes, including repressing stress responses
298 by inhibiting Rim15 via phosphorylation, which prevents it from activating Msn4 (Wanke *et al.*
299 2005, 2008). We hypothesized that Sch9 negatively regulates the ASR in *C. glabrata*. To test
300 this, we created a TORC1 phosphomimetic mutant of CgSch9, predicted to be constitutively
301 active with respect to TORC1 signaling (Urban *et al.* 2007) (Fig. S11). This mutant showed
302 reduced Cta1-GFP induction during phosphate starvation (Fig. 7E). Moreover, a quantitative
303 CFU assay failed to detect ASR in this mutant but did in the matching complement strain (Fig.
304 7F, raw $P = 0.69$ and 0.063, respectively), further supporting TORC1's role in the ASR.
305 Since TORC1 coordinates multiple cellular processes, we asked if phosphate starvation
306 had limited or broad effects on TORC1's downstream branches (Loewith and Hall 2011). To test
307 this, we monitored the Nitrogen Catabolism Repression (NCR) regulon, which is controlled by a
308 different branch, Tap42-PP2A, rather than by Sch9, and is differentially induced under nitrogen
309 starvation vs glucose starvation and other stresses in *S. cerevisiae* (Hughes Hallett *et al.* 2014).
310 Using an established *DAL80pr*-GFP reporter (Neklesa and Davis 2009), we found that nitrogen
311 starvation strongly induced NCR-sensitive genes, but phosphate starvation had minimal effects
312 in both *S. cerevisiae* and *C. glabrata* (Fig. S12). This suggests that evolution can wire an input
313 such as phosphate limitation to a specific TORC1 output, e.g., stress response, without strongly
314 impacting other outputs.

315 **Discussion**

316 Acquired stress resistance (ASR) is suggested to be an adaptive anticipatory response (Mitchell
317 *et al.* 2009). As such, it is expected to evolve between species. However, both the genetic basis
318 of ASR and its evolution remain poorly characterized. In this study, we discovered a divergent
319 ASR phenotype between two related yeasts: in the opportunistic pathogen, *C. glabrata*, a short,

320 non-lethal phosphate starvation provides a strong protective effect for a severe H_2O_2 stress,
321 while in the related baker's yeast, *S. cerevisiae*, the same treatment has little to no effect (Fig.
322 1). We identified a core subnetwork behind the ASR in *C. glabrata*, where phosphate starvation
323 not only induces the canonical phosphate starvation (PHO) response via the TF Pho4, but also
324 induces more than 15 oxidative stress response (OSR) genes, mediated by two TFs involved in
325 the canonical OSR, Msn4 and Skn7 (Fig. 2, 8A). Divergence in ASR between the two species is
326 due in part to the difference in nuclear translocation of Msn4 in response to phosphate
327 limitation. Remarkably, the central regulator TORC1 showed differential response to phosphate
328 in the two species while being similarly affected by nitrogen starvation (Fig. 7). This implicates
329 TORC1 as a key point of divergence behind the ASR evolution; it also shows how a conserved,
330 multifunctional complex can be evolutionarily tuned.
331 We showed that the divergence in the ASR for H_2O_2 between the two species is specific
332 to phosphate – two other primary stresses tested, glucose starvation and heat shock, elicit
333 similar protective effects in both species (Fig. S2). Why phosphate? Several lines of evidence
334 suggest that phosphate and genes involved in the PHO response are relevant in the host
335 environment, including impacting virulence in several infection models and affecting sensitivity
336 to ROS (Ikeh *et al.* 2017; Köhler *et al.* 2020). Moreover, while studies on the phagosome
337 environment mainly focused on nutrients such as glucose, a recent transcriptomic study showed
338 that PHO genes, such as the high affinity transporter *PHO84* and the secreted phosphatase
339 *PMU2* were both highly upregulated within 2 hours of *C. glabrata* being engulfed by human
340 macrophages (Fig. S13) (Rai *et al.* 2021). Conversely, we found that many genes induced when
341 *C. glabrata* cells were engulfed by macrophage were also induced during phosphate starvation,
342 including genes involved in autophagy, TCA cycle, amino acid biosynthesis and iron
343 homeostasis (Fig. S14). These results suggest that phosphate limitation is physiologically
344 relevant in the host and may serve as a stimulus to induce ASR for more severe stresses.
345 Does phosphate starvation provide general protection against any stress or is it specific
346 to certain types of stresses? We found that the protective effect of phosphate starvation varies
347 depending on the types of ROS used as the secondary stress (Fig. S3): the protective effect is
348 the strongest for H_2O_2, moderate for menadione sodium bisulfite, and non-existent for tBOOH.
349 The lack of ASR for tBOOH, an alkyl hydroperoxide, was initially surprising. However, this can
350 be understood based on its many differences from H_2O_2, e.g., its main cellular targets are lipids
351 in the plasma membrane; it reacts differently with the cellular redox system, and elicits different
352 signaling in *S. cerevisiae* than H_2O_2 (Iwai *et al.* 2010; Ikeda *et al.* 2011; Hajdu *et al.* 2021). This
353 demonstrates that ASR is specific to the primary and secondary stress combinations. We further
354 hypothesize that these combinations are frequently encountered in the organism's environment,
355 providing the selective pressure for the ASR.
356 The ASR effect in *C. glabrata* bears similarity to a previously described stress resistance
357 phenotype following chronic starvation in *S. cerevisiae* (Gresham *et al.* 2011; Petti *et al.* 2011;
358 Carter-O'Connell *et al.* 2012; Ebrahimi *et al.* 2021; Garg *et al.* 2023). Could the divergence in
359 ASR be attributed to the difference in timing/threshold of the chronic starvation response? We
360 think not. First, the chronic starvation response is associated with severe cell cycle arrests. We
361 found that during a short (< 2hrs) phosphate starvation, both species continue to divide with a

362 similar fraction of unbudded cells, suggesting that cell-cycle arrest cannot explain the species
363 difference in ASR (Fig. S15). Moreover, while several OSR genes were induced during chronic
364 phosphate starvation in *S. cerevisiae*, catalase genes were notably not among them (Petti *et al.*
365 2011). This is in contrast to the crucial role of *CTA1* induction for the ASR in *C. glabrata*. We
366 therefore believe that the phosphate starvation-induced ASR has distinct transcriptional basis
367 and serves a different purpose than the chronic starvation response.
368 Does ASR involve the same effector and regulator genes as the canonical response to
369 the secondary stress, or is it made up of an entirely different set of genes? We found phosphate
370 starvation-induced ASR in *C. glabrata* shares many of the TFs and effector genes with the
371 canonical OSR, but differs in the TF combinations required to induce the effector genes such as
372 *CTA1*, resulting in distinct induction kinetics (Fig. 2, 3, 8B). Such condition-specific regulation of
373 stress response genes has also been observed in *S. cerevisiae* and may be a hallmark of stress
374 response networks in general (Gasch *et al.* 2000). In theory, this could facilitate the evolution of
375 stress responses, including the ASR, by allowing for the reuse of existing genes and networks.
376 This likely depends on cis-regulatory mutations that modify the expression pattern of a gene in
377 one context with little or no impact under another, thereby reducing the pleiotropic effects.
378 Another intriguing finding is that the paralogous Msn2 and Msn4 showed divergent functions in
379 ASR and H_2O_2 stress between species. In *S. cerevisiae*, the two paralogs have largely identical
380 functions, with Msn2 playing a more important role (Berry and Gasch 2008; AkhavanAghdam *et*
381 *al.* 2016; Chapal *et al.* 2019; Wu *et al.* 2021). By contrast, Msn2 is dispensable for the induction
382 of *CTA1* in *C. glabrata* both during phosphate starvation and H_2O_2 stress, while Msn4 plays an
383 important role (Fig. 4, 5, S7). We speculate that the maintenance and evolution of TF paralogs
384 is an important source for ASR and, more generally, stress response evolution.
385 Lastly, given the central role and conservation of TORC1 across species, it is surprising
386 that its response to phosphate differed significantly between the two yeasts, which likely led to
387 their ASR divergence. How can a central, multi-functional regulator like TORC1 evolve? Our
388 results show that phosphate starvation specifically induced the stress response branch of
389 TORC1 while it had minimal effects on another branch associated with nitrogen catabolism (Fig.
390 7, S12). We propose that the ability to rewire specific input and output branches of TORC1
391 allows evolution to fine-tune the regulator's function without having pleiotropic effects (Fig. 8C).

392 **Materials and Methods**

393 **Experimental reproducibility and data availability**

394 Each experiment was repeated at least two but mostly three or more times with >2 biological
395 replicates each. Data analysis and visualization were performed in R v4.2. Raw data, R
396 markdown files, and output files are available at https://github.com/binhe-lab/E036-ASR-H2O2.
397 This repository will be version controlled by Zenodo upon publication.

398 **Yeast media and growth conditions**

399 Yeast cells were grown in the Yeast extract-Peptone Dextrose (YPD) medium or the Synthetic
400 Complete (SC), using Yeast Nitrogen Base without amino acids (Sigma Y0626) supplemented
401 with 2% glucose and amino acid mix. Unless specified, all stress treatments were performed
402 with mid-log phase cells. Briefly, cells were grown overnight in either YPD or SC media, diluted

403 in the morning to OD_{600} = 0.2 and grown to OD_{600} ~ 1. To apply the treatments, cells were
404 collected by centrifugation at 3,000g for 5 minutes, washed 2-3 times with water and released
405 into the treatment media. Nitrogen starvation medium was made using the Yeast Nitrogen Base
406 without amino acids and without ammonium sulfate (Sigma, Y1251). Glucose starvation medium
407 had 0.02% or 0.05% glucose in the SC medium. Phosphate starvation medium was made using
408 Yeast Nitrogen Base with ammonium sulfate, without phosphates, without sodium chloride (MP
409 Biomedicals, 114027812) and supplemented to a final concentration of 2% glucose, 1.5 mg/ml
410 potassium chloride, 0.1 mg/ml sodium chloride and amino acids, as described previously (He *et*
411 *al.* 2017). Phosphate concentration in the medium was measured using a Malachite Green
412 Phosphate Assay kit (Sigma, MAK307). The -MC medium used to induce *MET3pr-CTA1* was
413 made the same way as the SC medium, except methionine and cysteine were omitted from the
414 amino acid mix. To test the effect of inhibiting TORC1 on ASR, Rapamycin (RPI, R64500) was
415 added into the SC medium at the indicated concentrations. To apply H_2O_2 stress, H_2O_2 stock
416 solution (30% w/w, Sigma H1009) was diluted into SC medium to the indicated concentrations
417 immediately before the treatment, except in the *MET3pr-CTA1* experiment, where -MC medium
418 was used instead of SC medium to allow *CTA1* to be induced during the secondary stress. To
419 test additional ROS for the ASR effect, tert-butyl hydroperoxide (tBOOH 70% w/w in H_2O, Sigma
420 458139) was diluted directly into the SC medium, while menadione sodium bisulfite (Sigma
421 M5750) was first dissolved in ddH_2O to make a 1M stock, and then the stock was diluted into
422 the SC medium at the indicated concentrations immediately before the treatment.

423 **Generating yeast strains and plasmids**

424 Genetic transformation of both *S. cerevisiae* and *C. glabrata* was performed using the LiAc
425 method as described in (Gietz and Schiestl 2007). *C. glabrata* knockout strains were generated
426 with auxotrophic markers *HIS3* and *URA3* and the nourseothricin drug marker NAT. ~200 bp of
427 flanking homology sequences were added to either a deletion cassette or a knock-in construct
428 using overlap PCR. Transformants were confirmed by colony PCR on both sides of the gene.
429 To construct *CTA1* promoter mutants, a URA3 cassette was used to replace the endogenous
430 promoter, after which the mutant allele constructed by PCR mutagenesis was used as the repair
431 template to swap out the URA3 and selecting with 5-fluoroorotic acid (5-FOA) (GoldBio, F-320).
432 A similar approach was used to replace the endogenous *CTA1* promoter with the promoter from
433 the *C. glabrata MET3* gene. The *CgMET3* promoter was amplified from pCU-MET3 (Maroc and
434 Fairhead 2019) (AddGene #45336). The Msn2 and Msn4-GFP expression plasmids were made
435 by inserting the coding sequence of the genes in between the *PDC1* promoter and GFP in the
436 pCU-PDC1-GFP vector (Zordan *et al.* 2013) (AddGene #45342). The *ScDAL80*-GFP reporter
437 was constructed by amplifying the 1kb upstream region of *ScDAL80* and placing it in front of a
438 yeGFP in a pRS426 (ATCC #77107) backbone. Gibson cloning was performed according to the
439 protocol of the Gibson Assembly kit (NEB, E5520). To construct the Sch9-3E-NAT mutant and
440 the matching Sch9-WT-NAT control strains, we first used PCR-based mutagenesis to construct
441 the Sch9-3E fragment (Fig. S11). This and the Sch9-WT fragments were joined with the NAT
442 cassette via overlap PCR. Then, ~200bp of flanking sequences homologous to the endogenous
443 *SCH9* 5' and 3'UTR were added on both sides using overlap PCR. The end product was used
444 as a linear template to transform an *SCH9* wild type strain of *C. glabrata*. Positive transformants

445 were selected on YPD+NAT plates and validated by genomic PCR and sequencing. Yeast
446 strains, plasmids and qRT-PCR primers used in this study are listed in Table 1, Table 2 and
447 Table 3, respectively.

448 **Spotting and Colony Forming Units (CFU) assays**

449 A semi-quantitative spotting assay or a quantitative Colony Forming Unit (CFU) assay was used
450 to measure the survival rate after a treatment. For the spotting assay, the treated cells were 10x
451 serially diluted in ddH_2O. 5 µl of each dilution was spotted onto an SC plate and allowed to dry
452 before the plate was incubated at 30C for 16-36 hours. An image was taken at the end of the
453 incubation using a homemade imaging hood fitted with an iPad Air. For the CFU assay, post-
454 treatment cells were diluted 100 to 1,000-fold and plated on an SC plate. The dilution was
455 chosen to produce roughly 10-500 colonies per plate. The plates were incubated for 48 hours
456 and CFU was manually counted using a lab counter (Fisher Scientific).

457 **Calibrating H_2O_2 concentrations**

458 To apply an equivalent strength of H_2O_2 treatment to species and genotypes with different basal
459 survival rates, we measured the cell survival rates after treatment with different concentrations
460 of H_2O_2. Specifically, we exposed *S. cerevisiae* cells to a series of H_2O_2 concentrations from
461 0mM to 10mM, with 2mM steps. Similarly, we exposed *C. glabrata* cells H_2O_2 concentrations
462 from 0mM to 100mM with 20mM steps. CFU assays were performed after 2 hours of treatment
463 to estimate the survival rate. A Mann-Whitney U test was used to determine the significance of
464 differences. Concentrations resulting in similar survival rates across species or genotypes were
465 chosen as the condition for the secondary stress in the ASR experiment.

466 **Acquired stress resistance (ASR) assay**

467 During the primary stress phase, mid-log phase cells were collected, washed, and released into
468 either the SC medium for a mock treatment or the primary stress media, e.g., - Pi for phosphate
469 starvation. After 45 minutes (or as indicated) of incubation with shaking at 30 C, cells were
470 collected by centrifugation and resuspended at OD_{600} = 0.2 in the secondary stress treatment
471 media, then incubated the same as before for 2 hours. After the secondary stress, cells were
472 diluted and directly used for the spotting or CFU assay. CFU multiplied by the dilution rate was
473 then used to calculate r (MO/MM), r (PO/PM)' and the ASR-score (r'/r). Three to eight biological
474 replicates were performed.

475 **RNA-seq profiling for *C. glabrata* under phosphate starvation**

476 *C. glabrata* wild type cells were grown in SC overnight, diluted into fresh SC the next morning to
477 OD_{600} = 0.1, grown for another 2-3 hours until the culture reached mid-log phase (OD_{600}~0.6). At
478 this point, two biological replicates of pre-starvation samples were collected using a cold
479 methanol quenching method (Pieterse *et al.* 2006; Zhou and O'Shea 2011). Briefly, 5 mL of
480 culture was added directly into 7.5 mL of pre-chilled methanol (−50°C) and incubated in an
481 ethanol-dry ice bath at that temperature for at least 20 min. The remaining culture was collected
482 by filtration, washed with equal volume of pre-warmed no phosphate SC media and then
483 released into the pre-warmed no phosphate SC. After 1 hour incubation with shaking at 30 C,
484 three biological replicates of the starved samples were collected in the same way as above.
485 When all samples were in the ethanol-dry ice bath for > 20 minutes, cells were collected by

486 centrifugation and quickly washed with ice-cold water to remove the methanol and resuspended
487 in RNAlater solution (Qiagen, 76104) for at least 2 hours. Cells were centrifuged to remove the
488 RNAlater, flash-frozen in liquid nitrogen and stored at -80 C until RNA-extraction. For each
489 sample, ~$5x10^7$ cells were collected and total RNA was extracted using a MasterPure Yeast
490 RNA purification kit (Biosearch Technologies, MPY03100) following the manufacturer's protocol.
491 RNA-seq libraries were prepared with the TruSeq RNA Library Preparation Kit v2 (Illumina) with
492 the mRNA purification option. The resulting libraries were sequenced on an Illumina HiSeq
493 4000, which produced on average 10 million 50 bp single end reads for each sample.

494 **Comparing the transcriptional response to phosphate starvation between *C. glabrata* and**
495 ***S. cerevisiae***

496 The RNA-seq raw reads were mapped to the *C. glabrata* genome downloaded from the Candida
497 Genome Database (CGD, RRID:SCR_002036, version s02-m02-r09), using Bowtie v1.1.1
498 (RRID:SCR_005476) with the option '-m 1 --best –strata' (Langmead *et al.* 2009). The resulting
499 SAM files were sorted using Samtools v1.2 (RRID:SCR_002105) (Li *et al.* 2009) and the
500 number of reads per transcript was counted using Bedtools2 (RRID:SCR_006646) (Quinlan and
501 Hall 2010), with the option 'bedtools coverage -a BAM_file -b genome_annotation.bed -S -s
502 sorted -g Chrom.length`. Gene features for *C. glabrata* were downloaded from CGD, version
503 s02-m07-r04. The count matrix was filtered to remove lowly expressed genes (335 genes with
504 <1 read per sample on average). Next, we used the trimmed mean of M-values ('TMM') method
505 in the EdgeR (RRID:SCR_012802) package to calculate the normalization factors for scaling the
506 raw library sizes (Robinson *et al.* 2010), and applied voom transformation (Law *et al.* 2014) to
507 remove the mean-variance relationship on the log2 transformed count data. A log2 fold change
508 was calculated for each gene by subtracting the mean of the pre-starvation samples from each
509 of the 1-hr starvation sample values. For *S. cerevisiae*, the microarray data from (Zhou and
510 O'Shea 2011) was downloaded from the GEO database (RRID:SCR_005012). Within the series
511 GSE23580, three samples corresponding to the three biological replicates comparing the 1 hour
512 phosphate starved sample to a mock-treated sample were extracted (GSM578408, 578424,
513 578440). The log2 ratios were already background-subtracted, normalized, and used directly for
514 comparisons. To compare orthologous gene expression, we first curated a list of oxidative
515 stress response genes based on the literature (Table S1) (Lee *et al.* 1999; Hasan *et al.* 2002).
516 To identify their homologs in *C. glabrata*, we downloaded the orthology and best-hit mapping
517 between the two species from CGD. The best-hit mapping was based on less stringent criteria
518 and only used when an orthology mapping was not available. The resulting table of gene
519 expression log2 fold changes is available in Table S2.

520 ***CTA1* induction by quantitative real-time PCR (qRT-PCR)**

521 *C. glabrata* cells were mock-treated or treated with phosphate starvation or 1.5 mM H_2O_2 for 45
522 minutes. ~$2\text{-}4x10^7$ cells were harvested by centrifugation, snap-frozen in liquid nitrogen and
523 stored in -80 until RNA extraction. Two biological replicates were collected per condition. RNA
524 was extracted using a MasterPure Yeast RNA purification kit (Biosearch Technologies,
525 MPY03100). cDNA was synthesized using SuperScript™ III First-Strand Synthesis System
526 (Invitrogen, 18080051) and treated with RNase A (ThermoFisher, EN0531). We used the

527 LightCycler® 480 SYBR Green I Master (Roche, 04707516001) and qRT-PCR was performed
528 on a Roche LC480 instrument. Three technical replicates were performed for each sample. The
529 PCR program was 95°C for 5 minutes, followed by 45 cycles of 95°C for 10 seconds, 60°C for
530 20 seconds, and 72°C for 20 seconds. Data analysis was done using the instrument software,
531 including automatic baseline subtraction and C_T value quantifications. *ACT1* was used as a
532 reference gene and its C_T values were subtracted from those of *CTA1*. We then subtracted the
533 mean of the ΔC_T for the mock-treated samples from the technical replicates for the phosphate
534 starvation and H_2O_2-treated ones to obtain $\Delta\Delta C_T$, which were used for downstream analyses.

535 **Cta1-GFP time course by flow cytometry**

536 Cells were grown to mid-log phase in SC medium in 96 deep-well plates (VWR, 82051). After
537 washing with ddH_2O twice and spinning down at 3,000g for 5 minutes, cells were resuspended
538 in 0mM Pi SC medium, H_2O_2-containing SC medium or SC medium (7.5mM Pi), incubated at
539 30°C shaking at 200 rpm for 4 hrs. At the indicated time points, an aliquot of cell culture (40 -
540 50uL) was drawn and diluted into ddH_2O (360uL - 400uL) for flow cytometry on an Attune NxT
541 instrument fitted with an autosampler (Thermo Fisher). For each sample, 30,000 events were
542 recorded; non-cell events and doublets were removed based on FSC-H and FSC-W. Median
543 fluorescence intensity (MFI) was used for Cta1-GFP protein expression analysis.

544 **Binding site prediction for *CTA1* promoter**

545 To predict the binding sites (BS) for Skn7 and Msn4 in the *CgCTA1* promoter, we first retrieved
546 the 1000 bp DNA upstream of the start codon for the *CTA1* gene in the *C. glabrata* CBS138
547 genome (CGD, version s02-m02-r09). We then scanned this sequence with the expert curated
548 motifs for Skn7 and Msn4 from the Yetfasco (yetfasco.ccbr.utoronto.ca) database. To perform
549 the scanning, we first selected the two motifs for Skn7 and single expert curated motif for Msn4,
550 "added them to the cart", and used the "scan using cart" function. We adopted the default 75%
551 minimum percent of maximum score cutoff, and set the background percent A/T to 0.3, which
552 was based on the mean GC% in 1000 bp upstream sequences in the *C. glabrata* genome
553 calculated in-house. The motifs and prediction results were available in Supplementary Text S1.

554 **Fluorescent microscopy for Msn4 and Msn2 nuclear localization**

555 *C. glabrata* cells were transformed with the indicated plasmids and grown on SC Ura- plates for
556 selection. Transformed cells were then grown and maintained in SC Ura- liquid medium prior to
557 the experiments. *C. glabrata* cells were grown to mid-log phase in SC Ura- medium and treated
558 with SC, glucose starvation, or 0 mM Pi SC media for 30 mins. Subsequently, 4',6-diamidino-2-
559 phenylindole (DAPI, Sigma, D9542) was diluted in the respective medium and added to the
560 cultures at a final concentration of 10 ug/ml. Cells were incubated with DAPI in the dark for 15
561 minutes before DAPI was removed and cells were washed twice with ddH_2O. Finally, cells were
562 re-resuspended in the treatment medium. Fluorescent imaging was performed on a Leica SP8
563 confocal imaging system (Carver Center for Imaging, the University of Iowa). A 488 nm laser
564 was used for yeGFP excitation and 495-585 nm for emission; a 405 nm laser was used for DAPI
565 excitation and 430-550 nm for emission. In *S. cerevisiae*, Msn2-mCherry and Msn4-mCitrine
566 cells were prepared as described above excluding the DAPI staining. For Msn4-mCitrine, 488
567 nm was used for excitation and 501-547 nm for emission; for mCherry, 552 nm was used for

568 excitation and 570-649 nm for emission; for visualizing the nucleus with the Nhp6a-iRFP
569 marker, a 638 nm laser was used for excitation and 648-790 nm for emission.

570 **Total and P-Rps6 Western Blot**

571 Mid-log phase cells were subjected to either mock or starvation treatments in parallel. Cell lysis
572 buffer (0.1M NaOH, 0.05M EDTA, 2% SDS, 2% β-mercaptoethanol) and loading buffer (0.25M
573 Tris-HCL pH6.8, 50% Glycerol, 0.05% bromophenol blue) were prepared and protein extraction
574 was performed as described in (von der Haar 2007). Cell lysates were separated by SDS-PAGE
575 at 200 volts for 40 minutes, transferred onto nitrocellulose membranes (Bio-Rad, 1662807), and
576 stained with a total protein stain (Li-COR, 926-11015), which we used for normalization in place
577 of a loading control, as recommended by Li-COR. The membranes were blocked with 3% BSA
578 (RPI, A30075) at room temperature for 1 hr. Two blots for the same samples were probed with
579 either anti-phospho (Ser/Thr) Akt substrate rabbit polyclonal antibody (RRID:AB_330302, Cell
580 Signaling Technology # 9611) or Anti-RPS6 rabbit antibody (RRID:AB_945319, Abcam
581 ab40820) to detect the phosphorylated Rps6 (P-Rps6) and total S6, respectively. After washing,
582 the blots were incubated with a secondary antibody (RRID:AB_621843, LI-COR, 926-32211)
583 and imaged on a Li-COR Odyssey Fc scanner (Carver Center for Genomics, the University of
584 Iowa). The intensity of P-Rps6 and total Rps6 were quantified using the Li-COR Image Studio
585 software, following the manufacturer's instructions for the Revert™ 700 Total Protein Stain for
586 Western Blot Normalization. Briefly, the band of interest for each lane was selected using same-
587 sized rectangles. We then subtracted the background, calculated as the median of the top and
588 bottom regions of a band. We did the same analysis for the total protein stain image, except we
589 included the entire lane where bands are visible. We then normalized the Western blot signals
590 in each sample to the corresponding total protein stain to obtain the intensity for P-Rps6 or total
591 Rps6. Finally, we divided the two values to get the P-Rps6/total Rps6 ratio.

592 **Assaying cell morphology by light microscopy**

593 To determine the percent of unbudded cells during a phosphate starvation time course, wild
594 type *C. glabrata* and *S. cerevisiae* cells were grown as described above to mid-log phase,
595 collected by centrifugation, washed once with pre-warmed 0 mM Pi media and diluted to $5x10^6$
596 cells/mL in 0 mM Pi media. At 0, 20, 45, 75, 105 and 135 minutes into the time course, an
597 aliquot of cells was taken from each sample, sonicated for 5s to break up any cell clumps,
598 diluted 10-50x and counted on a hemocytometer (Marienfeld, 0640030) under a light
599 microscope. The number of unbudded cells over the total number of cells were recorded by
600 manually examining > 100 cells over four fields of view. The numbers from the four fields of
601 view were summed for downstream analysis.

602 **Statistical analyses and tests**

603 For <u>*quantitative ASR assays*</u> using CFU, the data from each replicate experiment was used to
604 calculate survival rates with or without the primary stress, expressed as $r = CFU_{MO} / CFU_{MM}$ and
605 $r' = CFU_{PO} / CFU_{PM}$. The fold change in survival due to the primary stress, expressed as r'/r, aka
606 ASR-score, was calculated for each experiment. We estimated the mean and 95% confidence
607 interval for the ASR-score with 1000 bootstraps using the smean.cl.boot() function in the Hmisc
608 package. To identify equivalent strengths of ROS for different species and strains, a Mann-

Whitney U test was used to test for differences in the basal survival rates (r) and a two-sided *P*-value was reported. To assess the statistical significance of the ASR effect in a strain, we used the paired r and r' estimates from each replicate and performed a Wilcoxon signed-rank test if n >= 4. When n < 4, a paired Student's t-test was used since the former test has very low power at such a small sample size. The one-sided *P*-value, with the alternative hypothesis being r' > r, was reported in the legend and text. To compare the ASR effect sizes between two strains, a Mann-Whitney U test (aka Wilcoxson rank-sum test) was performed for the paired data. A two-sided *P*-value was reported. When more than one comparison was made, a Bonferroni correction was applied. For *transcriptomic comparisons*, we performed a t-test for the triplicates of the log2 fold changes for 29 genes in both species. The alternative hypothesis was that the true log2 fold change was greater than 0 (induced under phosphate starvation). The resulting *P*-values were adjusted for multiple comparisons using the Benjamini-Hochberg procedure (FDR). Genes with an FDR < 0.05 and a log2 fold change > 2 were considered significantly induced. For *CTA1 induction by qRT-PCR*, the $\Delta\Delta C_T$ values from the three technical replicates for the phosphate starved, H_2O_2-treated and mock-treated samples were analyzed using a linear model, with the two stress conditions treated as dummy variables and the biological replicate included as a covariate (R: lm(ddCt ~ treatment + strain), where treatment is a factor with levels = {"Mock", "-Pi", "H_2O_2"}). Raw *P*-values for each level were reported. For Cta1-GFP basal and induced levels, a linear model was used to compare the different genotypes and the *P*-values were Bonferroni-corrected (multiplied by 5 mutants). For *Msn4 nuclear localization*, cells with nuclear-localized vs cytoplasmic Msn4 were counted under a fluorescent microscope (>100 cells in total per strain x condition). A Fisher's Exact Test (FET) was performed for cells with or without nuclear-localized Msn4 and between species/genotypes. *P*-values were calculated using an exact method. When multiple comparisons were made, a Bonferroni correction was applied unless otherwise noted in the text or legend. For *Western Blot analysis of P-Rps6 / total Rps6*, the samples being compared were run on the same gel for each replicate. Thus, a paired Student's t-test was performed, and a two-sided *P*-values after Bonferroni correction was used to assess the significance of the difference between the treatment conditions.

Acknowledgement

We would like to thank Lan Qing and Chris Koon Ho Wong for kindly providing the PolII ChIP-seq data for phagocytosed *C. glabrata*. We would like to thank Dr. Nan Hao for sending us the *S. cerevisiae* Msn2 and Msn4 fluorescently tagged strains. We thank Dr. Anthony Pannullo and other members of the Gene Regulatory Lab members for reading and giving feedback on the manuscript. We also want to thank Drs. Daniel Summers, Damian Krysan, Josep Comeron and Andrew Capaldi for giving suggestions on the work. Drs. Jan Fassler, Veena Prahlad and Bing Luan read an early draft of the paper and gave valuable feedback. Lastly, we would like to thank the editor and three anonymous reviewers for improving the manuscript.

Funding

Dr. Bin Z. He is supported by NIH R35GM137831 and a start-up fund provided by the University of Iowa.

649 **Literature Cited**

650 AkhavanAghdam Z., J. Sinha, O. P. Tabbaa, and N. Hao, 2016 Dynamic control of gene
651 regulatory logic by seemingly redundant transcription factors. eLife 5: e18458.
652 https://doi.org/10.7554/eLife.18458

653 Beck T., and M. N. Hall, 1999 The TOR signalling pathway controls nuclear localization of
654 nutrient-regulated transcription factors. Nature 402: 689–692. https://doi.org/10.1038/45287

655 Berry D. B., and A. P. Gasch, 2008 Stress-activated Genomic Expression Changes Serve a
656 Preparative Role for Impending Stress in Yeast. Mol. Biol. Cell 19: 4580–4587.
657 https://doi.org/10.1091/mbc.E07-07-0680

658 Berry D. B., Q. Guan, J. Hose, S. Haroon, M. Gebbia, *et al.*, 2011 Multiple means to the same
659 end: the genetic basis of acquired stress resistance in yeast. PLoS Genet. 7: e1002353.
660 https://doi.org/10.1371/journal.pgen.1002353

661 Boisnard S., G. Lagniel, C. Garmendia-Torres, M. Molin, E. Boy-Marcotte, *et al.*, 2009 H2O2
662 Activates the Nuclear Localization of Msn2 and Maf1 through Thioredoxins in Saccharomyces
663 cerevisiae. Eukaryot. Cell 8: 1429. https://doi.org/10.1128/EC.00106-09

664 Brown A. J. P., D. E. Larcombe, and A. Pradhan, 2020 Thoughts on the evolution of Core
665 Environmental Responses in yeasts. Fungal Biol. 124: 475–481.
666 https://doi.org/10.1016/j.funbio.2020.01.003

667 Brunke S., and B. Hube, 2013 Two unlike cousins: Candida albicans and C. glabrata infection
668 strategies. Cell. Microbiol. 15: 701–708. https://doi.org/10.1111/cmi.12091

669 Carter-O'Connell I., M. T. Peel, D. D. Wykoff, and E. K. O'Shea, 2012 Genome-wide
670 characterization of the phosphate starvation response in Schizosaccharomyces pombe. BMC
671 Genomics 13: 697. https://doi.org/10.1186/1471-2164-13-697

672 Chapal M., S. Mintzer, S. Brodsky, M. Carmi, and N. Barkai, 2019 Resolving noise-control
673 conflict by gene duplication. PLoS Biol. 17: e3000289.
674 https://doi.org/10.1371/journal.pbio.3000289

675 Chen D., W. M. Toone, J. Mata, R. Lyne, G. Burns, *et al.*, 2003 Global transcriptional responses
676 of fission yeast to environmental stress. Mol. Biol. Cell 14: 214–229.
677 https://doi.org/10.1091/mbc.E02-08-0499

678 Cormack B. P., and S. Falkow, 1999 Efficient homologous and illegitimate recombination in the
679 opportunistic yeast pathogen Candida glabrata. Genetics 151: 979–987.

680 Cuéllar-Cruz M., M. Briones-Martin-del-Campo, I. Cañas-Villamar, J. Montalvo-Arredondo, L.
681 Riego-Ruiz, *et al.*, 2008 High Resistance to Oxidative Stress in the Fungal Pathogen Candida
682 glabrata Is Mediated by a Single Catalase, Cta1p, and Is Controlled by the Transcription Factors
683 Yap1p, Skn7p, Msn2p, and Msn4p. Eukaryot. Cell 7: 814–825.
684 https://doi.org/10.1128/EC.00011-08

685 Davies K. J. A., 2016 Adaptive homeostasis. Mol. Aspects Med. 49: 1–7.
686 https://doi.org/10.1016/j.mam.2016.04.007

687 Dujon B., D. Sherman, G. Fischer, P. Durrens, S. Casaregola, *et al.*, 2004 Genome evolution in
688 yeasts. Nature 430: 35–44. https://doi.org/10.1038/nature02579

Durrant W. E., and X. Dong, 2004 Systemic acquired resistance. Annu. Rev. Phytopathol. 42: 185–209. https://doi.org/10.1146/annurev.phyto.42.040803.140421

Ebrahimi M., L. Habernig, F. Broeskamp, A. Aufschnaiter, J. Diessl, *et al.*, 2021 Phosphate Restriction Promotes Longevity via Activation of Autophagy and the Multivesicular Body Pathway. Cells 10. https://doi.org/10.3390/cells10113161

Fidel P. L., J. A. Vazquez, and J. D. Sobel, 1999 Candida glabrata: Review of Epidemiology, Pathogenesis, and Clinical Disease with Comparison to C. albicans. Clin. Microbiol. Rev. 12: 80–96.

Garg A., A. M. Sanchez, M. Miele, B. Schwer, and S. Shuman, 2023 Cellular responses to long-term phosphate starvation of fission yeast: Maf1 determines fate choice between quiescence and death associated with aberrant tRNA biogenesis. Nucleic Acids Res. gkad063. https://doi.org/10.1093/nar/gkad063

Gasch A. P., P. T. Spellman, C. M. Kao, O. Carmel-Harel, M. B. Eisen, *et al.*, 2000 Genomic expression programs in the response of yeast cells to environmental changes. Mol. Biol. Cell 11: 4241–4257.

Gietz R. D., and R. H. Schiestl, 2007 High-efficiency yeast transformation using the LiAc/SS carrier DNA/PEG method. Nat. Protoc. 2: 31–34. https://doi.org/10.1038/nprot.2007.13

González A., M. Shimobayashi, T. Eisenberg, D. A. Merle, T. Pendl, *et al.*, 2015 TORC1 Promotes Phosphorylation of Ribosomal Protein S6 via the AGC Kinase Ypk3 in Saccharomyces cerevisiae. PLOS ONE 10: e0120250. https://doi.org/10.1371/journal.pone.0120250

Görner W., E. Durchschlag, M. T. Martinez-Pastor, F. Estruch, G. Ammerer, *et al.*, 1998 Nuclear localization of the C2H2 zinc finger protein Msn2p is regulated by stress and protein kinase A activity. Genes Dev. 12: 586–597. https://doi.org/10.1101/gad.12.4.586

Goulev Y., S. Morlot, A. Matifas, B. Huang, M. Molin, *et al.*, 2017 Nonlinear feedback drives homeostatic plasticity in H2O2 stress response. eLife 6: e23971. https://doi.org/10.7554/eLife.23971

Gresham D., V. M. Boer, A. Caudy, N. Ziv, N. J. Brandt, *et al.*, 2011 System-level analysis of genes and functions affecting survival during nutrient starvation in Saccharomyces cerevisiae. Genetics 187: 299–317. https://doi.org/10.1534/genetics.110.120766

Haar T. von der, 2007 Optimized protein extraction for quantitative proteomics of yeasts. PloS One 2: e1078. https://doi.org/10.1371/journal.pone.0001078

Hajdu T., K. Szabó, Á. Jakab, I. Pócsi, V. Dombrádi, *et al.*, 2021 Biophysical experiments reveal a protective role of protein phosphatase Z1 against oxidative damage of the cell membrane in Candida albicans. Free Radic. Biol. Med. 176: 222–227. https://doi.org/10.1016/j.freeradbiomed.2021.09.020

Hasan R., C. Leroy, A.-D. Isnard, J. Labarre, E. Boy-Marcotte, *et al.*, 2002 The control of the yeast H2O2 response by the Msn2/4 transcription factors. Mol. Microbiol. 45: 233–241. https://doi.org/10.1046/j.1365-2958.2002.03011.x

He B. Z., X. Zhou, and E. K. O'Shea, 2017 Evolution of reduced co-activator dependence led to target expansion of a starvation response pathway. eLife 6. https://doi.org/10.7554/eLife.25157

730 Hecker M., J. Pané-Farré, and U. Völker, 2007 SigB-dependent general stress response in
731 Bacillus subtilis and related gram-positive bacteria. Annu. Rev. Microbiol. 61: 215–236.
732 https://doi.org/10.1146/annurev.micro.61.080706.093445

733 Hughes Hallett J. E., X. Luo, and A. P. Capaldi, 2014 State transitions in the TORC1 signaling
734 pathway and information processing in Saccharomyces cerevisiae. Genetics 198: 773–786.
735 https://doi.org/10.1534/genetics.114.168369

736 Ikeda Y., M. Nakano, H. Ihara, R. Ito, N. Taniguchi, *et al.*, 2011 Different consequences of
737 reactions with hydrogen peroxide and t-butyl hydroperoxide in the hyperoxidative inactivation of
738 rat peroxiredoxin-4. J. Biochem. (Tokyo) 149: 443–453. https://doi.org/10.1093/jb/mvq156

739 Ikeh M. A. C., S. L. Kastora, A. M. Day, C. M. Herrero-de-Dios, E. Tarrant, *et al.*, 2016 Pho4
740 mediates phosphate acquisition in Candida albicans and is vital for stress resistance and metal
741 homeostasis. Mol. Biol. Cell mbc.E16-05-0266. https://doi.org/10.1091/mbc.E16-05-0266

742 Ikeh M., Y. Ahmed, and J. Quinn, 2017 Phosphate Acquisition and Virulence in Human Fungal
743 Pathogens. Microorganisms 5. https://doi.org/10.3390/microorganisms5030048

744 Iwai K., A. Naganuma, and S. Kuge, 2010 Peroxiredoxin Ahp1 acts as a receptor for
745 alkylhydroperoxides to induce disulfide bond formation in the Cad1 transcription factor. J. Biol.
746 Chem. 285: 10597–10604. https://doi.org/10.1074/jbc.M109.090142

747 Jamieson D. J., 1998 Oxidative stress responses of the yeast Saccharomyces cerevisiae. Yeast
748 14: 1511–1527. https://doi.org/10.1002/(SICI)1097-0061(199812)14:16<1511::AID-
749 YEA356>3.0.CO;2-S

750 Köhler J. R., M. Acosta-Zaldívar, and W. Qi, 2020 Phosphate in Virulence of Candida albicans
751 and Candida glabrata. J. Fungi Basel Switz. 6: E40. https://doi.org/10.3390/jof6020040

752 Kumar K., F. Askari, M. S. Sahu, and R. Kaur, 2019 Candida glabrata: A Lot More Than Meets
753 the Eye. Microorganisms 7: 39. https://doi.org/10.3390/microorganisms7020039

754 Langmead B., C. Trapnell, M. Pop, and S. L. Salzberg, 2009 Ultrafast and memory-efficient
755 alignment of short DNA sequences to the human genome. Genome Biol. 10: R25.
756 https://doi.org/10.1186/gb-2009-10-3-r25

757 Law C. W., Y. Chen, W. Shi, and G. K. Smyth, 2014 voom: precision weights unlock linear
758 model analysis tools for RNA-seq read counts. Genome Biol. 15: R29.
759 https://doi.org/10.1186/gb-2014-15-2-r29

760 Lee J., C. Godon, G. Lagniel, D. Spector, J. Garin, *et al.*, 1999 Yap1 and Skn7 Control Two
761 Specialized Oxidative Stress Response Regulons in Yeast. J. Biol. Chem. 274: 16040–16046.
762 https://doi.org/10.1074/jbc.274.23.16040

763 Lee P., M. S. Kim, S.-M. Paik, S.-H. Choi, B.-R. Cho, *et al.*, 2013 Rim15-dependent activation of
764 Hsf1 and Msn2/4 transcription factors by direct phosphorylation in Saccharomyces cerevisiae.
765 FEBS Lett. 587: 3648–3655. https://doi.org/10.1016/j.febslet.2013.10.004

766 Leroi A. M., A. F. Bennett, and R. E. Lenski, 1994 Temperature acclimation and competitive
767 fitness: an experimental test of the beneficial acclimation assumption. Proc. Natl. Acad. Sci. U.
768 S. A. 91: 1917–1921. https://doi.org/10.1073/pnas.91.5.1917

769 Lev S., K. Kaufman-Francis, D. Desmarini, P. G. Juillard, C. Li, *et al.*, 2017 Pho4 Is Essential for
770 Dissemination of Cryptococcus neoformans to the Host Brain by Promoting Phosphate Uptake
771 and Growth at Alkaline pH. mSphere 2. https://doi.org/10.1128/mSphere.00381-16

772 Li H., B. Handsaker, A. Wysoker, T. Fennell, J. Ruan, *et al.*, 2009 The Sequence
773 Alignment/Map format and SAMtools. Bioinforma. Oxf. Engl. 25: 2078–2079.
774 https://doi.org/10.1093/bioinformatics/btp352

775 Liu N.-N., P. R. Flanagan, J. Zeng, N. M. Jani, M. E. Cardenas, *et al.*, 2017 Phosphate is the
776 third nutrient monitored by TOR in Candida albicans and provides a target for fungal-specific
777 indirect TOR inhibition. Proc. Natl. Acad. Sci. 114: 6346–6351.
778 https://doi.org/10.1073/pnas.1617799114

779 Liu N.-N., P. Uppuluri, A. Broggi, A. Besold, K. Ryman, *et al.*, 2018 Intersection of phosphate
780 transport, oxidative stress and TOR signalling in Candida albicans virulence. PLOS Pathog. 14:
781 e1007076. https://doi.org/10.1371/journal.ppat.1007076

782 Loewith R., and M. N. Hall, 2011 Target of rapamycin (TOR) in nutrient signaling and growth
783 control. Genetics 189: 1177–1201. https://doi.org/10.1534/genetics.111.133363

784 Lou Y., and A. E. Yousef, 1997 Adaptation to sublethal environmental stresses protects Listeria
785 monocytogenes against lethal preservation factors. Appl. Environ. Microbiol. 63: 1252–1255.
786 https://doi.org/10.1128/aem.63.4.1252-1255.1997

787 Lu D., N. Maulik, I. I. Moraru, D. L. Kreutzer, and D. K. Das, 1993 Molecular adaptation of
788 vascular endothelial cells to oxidative stress. Am. J. Physiol. 264: C715-722.
789 https://doi.org/10.1152/ajpcell.1993.264.3.C715

790 Magnuson B., B. Ekim, and D. C. Fingar, 2012 Regulation and function of ribosomal protein S6
791 kinase (S6K) within mTOR signalling networks. Biochem. J. 441: 1–21.
792 https://doi.org/10.1042/BJ20110892

793 Maroc L., and C. Fairhead, 2019 A new inducible CRISPR-Cas9 system useful for genome
794 editing and study of DSB repair in Candida glabrata. Yeast Chichester Engl.
795 https://doi.org/10.1002/yea.3440

796 Mason D. A., N. Shulga, S. Undavai, E. Ferrando-May, M. F. Rexach, *et al.*, 2005 Increased
797 nuclear envelope permeability and Pep4p-dependent degradation of nucleoporins during
798 hydrogen peroxide-induced cell death. FEMS Yeast Res. 5: 1237–1251.
799 https://doi.org/10.1016/j.femsyr.2005.07.008

800 Mitchell A., G. H. Romano, B. Groisman, A. Yona, E. Dekel, *et al.*, 2009 Adaptive prediction of
801 environmental changes by microorganisms. Nature 460: 220–224.
802 https://doi.org/10.1038/nature08112

803 Neklesa T. K., and R. W. Davis, 2009 A Genome-Wide Screen for Regulators of TORC1 in
804 Response to Amino Acid Starvation Reveals a Conserved Npr2/3 Complex. PLOS Genet. 5:
805 e1000515. https://doi.org/10.1371/journal.pgen.1000515

806 Nikolaou E., I. Agrafioti, M. Stumpf, J. Quinn, I. Stansfield, *et al.*, 2009 Phylogenetic diversity of
807 stress signalling pathways in fungi. BMC Evol. Biol. 9: 44. https://doi.org/10.1186/1471-2148-9-
808 44

809 Pedruzzi I., F. Dubouloz, E. Cameroni, V. Wanke, J. Roosen, *et al.*, 2003 TOR and PKA
810 signaling pathways converge on the protein kinase Rim15 to control entry into G0. Mol. Cell 12:
811 1607–1613. https://doi.org/10.1016/s1097-2765(03)00485-4

812 Petti A. A., C. A. Crutchfield, J. D. Rabinowitz, and D. Botstein, 2011 Survival of starving yeast
813 is correlated with oxidative stress response and nonrespiratory mitochondrial function. Proc.
814 Natl. Acad. Sci. 108: E1089–E1098. https://doi.org/10.1073/pnas.1101494108

815 Pieterse B., R. H. Jellema, and M. J. van der Werf, 2006 Quenching of microbial samples for
816 increased reliability of microarray data. J. Microbiol. Methods 64: 207–216.
817 https://doi.org/10.1016/j.mimet.2005.04.035

818 Plank M., 2022 Interaction of TOR and PKA Signaling in S. cerevisiae. Biomolecules 12: 210.
819 https://doi.org/10.3390/biom12020210

820 Quinlan A. R., and I. M. Hall, 2010 BEDTools: a flexible suite of utilities for comparing genomic
821 features. Bioinformatics 26: 841–842. https://doi.org/10.1093/bioinformatics/btq033

822 Rai M. N., C. Parsania, R. Rai, N. Shirgaonkar, K. Tan, *et al.*, 2021 Temporal transcriptional
823 response of Candida glabrata during macrophage infection reveals a multifaceted transcriptional
824 regulator CgXbp1 important for macrophage response and drug resistance. 2021.09.28.462173.

825 Reichmann D., W. Voth, and U. Jakob, 2018 Maintaining a Healthy Proteome during Oxidative
826 Stress. Mol. Cell 69: 203–213. https://doi.org/10.1016/j.molcel.2017.12.021

827 Rhind N., Z. Chen, M. Yassour, D. A. Thompson, B. J. Haas, *et al.*, 2011 Comparative
828 Functional Genomics of the Fission Yeasts. Science 332: 930–936.
829 https://doi.org/10.1126/science.1203357

830 Robinson M. D., D. J. McCarthy, and G. K. Smyth, 2010 edgeR: a Bioconductor package for
831 differential expression analysis of digital gene expression data. Bioinformatics 26: 139–140.
832 https://doi.org/10.1093/bioinformatics/btp616

833 Rodaki A., I. M. Bohovych, B. Enjalbert, T. Young, F. C. Odds, *et al.*, 2009 Glucose promotes
834 stress resistance in the fungal pathogen Candida albicans. Mol. Biol. Cell 20: 4845–4855.
835 https://doi.org/10.1091/mbc.e09-01-0002

836 Roetzer A., C. Gregori, A. M. Jennings, J. Quintin, D. Ferrandon, *et al.*, 2008 Candida glabrata
837 environmental stress response involves Saccharomyces cerevisiae Msn2/4 orthologous
838 transcription factors. Mol. Microbiol. 69: 603–620. https://doi.org/10.1111/j.1365-
839 2958.2008.06301.x

840 Romanowski K., A. Zaborin, V. Valuckaite, R. J. Rolfes, T. Babrowski, *et al.*, 2012 Candida
841 albicans Isolates from the Gut of Critically Ill Patients Respond to Phosphate Limitation by
842 Expressing Filaments and a Lethal Phenotype, (N. Chauhan, Ed.). PLoS ONE 7: e30119.
843 https://doi.org/10.1371/journal.pone.0030119

844 Scholz H., M. Franz, and U. Heberlein, 2005 The hangover gene defines a stress pathway
845 required for ethanol tolerance development. Nature 436: 845–847.
846 https://doi.org/10.1038/nature03864

847 Seider K., F. Gerwien, L. Kasper, S. Allert, S. Brunke, *et al.*, 2014 Immune Evasion, Stress
848 Resistance, and Efficient Nutrient Acquisition Are Crucial for Intracellular Survival of Candida
849 glabrata within Macrophages. Eukaryot. Cell 13: 170–183. https://doi.org/10.1128/EC.00262-13

850 Shen X.-X., D. A. Opulente, J. Kominek, X. Zhou, J. L. Steenwyk, *et al.*, 2018 Tempo and Mode
851 of Genome Evolution in the Budding Yeast Subphylum. Cell 175: 1533–1545.
852 https://doi.org/10.1016/j.cell.2018.10.023

853 Swinnen E., V. Wanke, J. Roosen, B. Smets, F. Dubouloz, *et al.*, 2006 Rim15 and the
854 crossroads of nutrient signalling pathways in Saccharomyces cerevisiae. Cell Div. 1: 3.
855 https://doi.org/10.1186/1747-1028-1-3

856 Urban J., A. Soulard, A. Huber, S. Lippman, D. Mukhopadhyay, *et al.*, 2007 Sch9 is a major
857 target of TORC1 in Saccharomyces cerevisiae. Mol. Cell 26: 663–674.
858 https://doi.org/10.1016/j.molcel.2007.04.020

859 Wanke V., I. Pedruzzi, E. Cameroni, F. Dubouloz, and C. De Virgilio, 2005 Regulation of G0
860 entry by the Pho80-Pho85 cyclin-CDK complex. EMBO J. 24: 4271–4278.
861 https://doi.org/10.1038/sj.emboj.7600889

862 Wanke V., E. Cameroni, A. Uotila, M. Piccolis, J. Urban, *et al.*, 2008 Caffeine extends yeast
863 lifespan by targeting TORC1. Mol. Microbiol. 69: 277–285. https://doi.org/10.1111/j.1365-
864 2958.2008.06292.x

865 Welker S., B. Rudolph, E. Frenzel, F. Hagn, G. Liebisch, *et al.*, 2010 Hsp12 is an intrinsically
866 unstructured stress protein that folds upon membrane association and modulates membrane
867 function. Mol. Cell 39: 507–520. https://doi.org/10.1016/j.molcel.2010.08.001

868 Wu Y., J. Wu, M. Deng, and Y. Lin, 2021 Yeast cell fate control by temporal redundancy
869 modulation of transcription factor paralogs. Nat. Commun. 12: 3145.
870 https://doi.org/10.1038/s41467-021-23425-0

871 Zakhem A. E., R. Istambouli, M. Alkozah, A. Gharamti, M. A. Tfaily, *et al.*, 2021 Predominance
872 of Candida Glabrata among Non-albicans Candida Species in a 16-Year Study of Candidemia
873 at a Tertiary Care Center in Lebanon. Pathog. Basel Switz. 10.
874 https://doi.org/10.3390/pathogens10010082

875 Zhou X., and E. K. O'Shea, 2011 Integrated approaches reveal determinants of genome-wide
876 binding and function of the transcription factor Pho4. Mol. Cell 42: 826–836.
877 https://doi.org/10.1016/j.molcel.2011.05.025

878 Zordan R. E., Y. Ren, S.-J. Pan, G. Rotondo, A. D. L. Peñas, *et al.*, 2013 Expression Plasmids
879 for Use in Candida glabrata. G3 GenesGenomesGenetics 3: 1675–1686.
880 https://doi.org/10.1534/g3.113.006908

881

882 **Figure Legends**

883 **Figure 1. Phosphate starvation induces strong acquired resistance for H_2O_2 in *C. glabrata***
884 **and not in *S. cerevisiae*.** (A) Experimental design for quantifying Acquired Stress Resistance
885 (ASR): cells were first treated with phosphate starvation (-Pi, or P) or mock-treated (M), then
886 exposed to a secondary H_2O_2 (O) stress or a mock treatment (M). The resulting treatment
887 regimens were referred to as PO, MO, PM and MM. After each treatment regimen, *C. glabrata*
888 (B) and *S. cerevisiae* (C) cells were spotted on rich solid media and imaged after 24-48 hrs.
889 Different H_2O_2 concentrations were used for the two species to achieve a similar survival rate

890 without the primary stress. (D) Survival rates (%) after the secondary H_2O_2 challenge were
891 quantified using Colony Forming Units either with (r') or without (r) phosphate starvation as a
892 primary stress. The biological replicates (n=8) were shown as dots and their means as bars. Basal
893 survival rates (r) were not different between species (*P* = 0.38), while there was a significant
894 increase in survival due to the primary stress in *C. glabrata* but not in *S. cerevisiae* (*P*-values =
895 0.0039 and 0.37, respectively).
896
897 **Figure 2. Phosphate starvation strongly induces many oxidative stress related genes in *C.***
898 ***glabrata* but not in *S. cerevisiae*.** (A) Proposed transcriptional basis for the acquired stress
899 resistance in *C. glabrata*: phosphate starvation induces both canonical phosphate homeostasis
900 genes and also oxidative stress response genes, providing protection for the secondary H_2O_2
901 challenge. (B-E) Comparison of transcriptional induction of genes known to be involved in OSR
902 in *S. cerevisiae*. Log2 fold changes after 1 hour of phosphate starvation were shown as the mean
903 (bar) of 3 biological replicates (dots) for genes encoding antioxidants (B), protease components
904 (C), molecular chaperones (D) and TFs involved in the OSR (E). The dotted lines indicate a 2 fold
905 induction. Gene names were based on *S. cerevisiae* except for *CTA1*, which had two paralogs in
906 *S. cerevisiae* and only one in *C. glabrata*. *S. cerevisiae CTT1* is involved in OSR and its fold
907 change is shown in (B). Asterisks above a gene name indicate that the gene was significantly
908 induced in that species at an FDR of 0.05.
909
910 **Figure 3. *C. glabrata CTA1* is induced during phosphate starvation and is required for the**
911 **acquired resistance to severe H_2O_2 stress.** (A) *CTA1* mRNA levels were assayed using qRT-
912 PCR following 45 minutes of either 1.5 mM H_2O_2, phosphate starvation or mock treatment. Fold
913 changes over the mock treated samples were shown using *ACT1* as a reference. Two isogenic
914 lab strains of *C. glabrata* were each assayed in triplicates. Bars represent the mean of each strain.
915 An unpaired Student's t-test comparing the $\Delta\Delta C_T$ values between both treatments with the mock
916 found both to be significantly elevated ($P < 0.01$, strain was included as a covariate and found to
917 be not significant). (B) Cta1 protein levels were monitored in strains carrying a genomic *CTA*1-
918 GFP fusion using flow cytometry for 4 hours, during which cells were exposed to either mild H_2O_2
919 stress, phosphate starvation or mock treatment. The y-axis values are the median fluorescence
920 intensities (a.u. = arbitrary unit). The dots show the mean of >3 biological replicates; the error
921 bars show 95% confidence intervals based on bootstrapping and the lines are LOESS curves
922 fitted to the data. (C) ASR spotting assays for wild type and *cta1*Δ *C. glabrata* strains. 2.5 mM
923 H_2O_2 was used as the secondary stress for *cta1*Δ, which resulted in a similar basal survival rate
924 as 100 mM H_2O_2 for the wild type. (D) ASR effects were quantified by comparing the survival rates
925 after H2O2 treatments either with (solid circles) or without (open circles) the primary stress using
926 a colony forming unit (CFU) assay. The difference in basal survival rates was not statistically
927 significant between the wild type and the *cta1*Δ strain (*P* = 0.39). Phosphate starvation
928 significantly increased the survival of both strains during the secondary challenge (raw *P* = 0.016
929 in both), but the ASR effect size was much smaller in cta1Δ (ASR-score = 9.8 and 1.5 in wild type
930 and *cta1*Δ, respectively; Mann-Whitney U test *P* = 0.001 between the two).
931

932 **Figure 4. TFs CgMsn4 and CgSkn7 jointly contribute to *CTA1* induction during phosphate**
933 **starvation in *C. glabrata*.** (A) Cta1-GFP levels over 4 hours of phosphate starvation for wild type
934 (WT) and TF deletion mutants. The dots represent the mean of > 3 biological replicates and the
935 error bars indicate the 95% confidence interval based on 1000 bootstrap replicates. The lines are
936 LOESS fit to the data. (B) A schematic showing the predicted binding sites (BS) for Skn7 and
937 Msn2/Msn4 in *C. glabrata* (Materials and Methods). Based on the prediction, two types of *cis*-
938 mutants were created: the internal deletions (4OL, 8OL) each removed 200 bp containing either
939 the predicted Msn2/Msn4 BS or both Skn7 BS; four point mutation alleles each targeted either
940 the single Msn2/Msn4 BS or one of the Skn7 BS predicted to have a higher affinity. (C, D)
941 Comparing the Cta1-GFP induction driven by each of the mutant promoters in (B) compared with
942 the WT and the corresponding TF∆ mutant.
943
944 **Figure 5. *C. glabrata* Msn4 (CgMsn4) translocates into the nucleus upon phosphate**
945 **starvation but not its ortholog in *S. cerevisiae* (ScMsn4).** Cellular localization of CgMsn4 (A)
946 and ScMsn4 (B) under phosphate starvation (0 mM Pi, -Pi), glucose starvation (0.02% glucose, -
947 Glu), and no stress conditions. All treatments were for 45 minutes. From left to right: i. CgMsn4-
948 yeGFP and ScMsn4-mCitrine; ii. nucleus staining with DAPI in *C. glabrata* or labeled with Nh6a-
949 iRFP in *S. cerevisiae*; iii. merge; iv. bright field. The percent of cells with nuclear-localized Msn4
950 and the total number of cells examined by microscopy were shown on the right. Scale bars are 5
951 µm in length.
952
953 **Figure 6. The Greatwall kinase homolog Rim15 mediates phosphate starvation-induced**
954 **ASR in *C. glabrata*.** (A) Proposed model for phosphate starvation-induced ASR in *C. glabrata*:
955 phosphate starvation (-Pi) activates Rim15, which goes on to regulate Msn4's activity and
956 contributes to ASR. Dashed arrows show proposed connections; solid arrows are regulations
957 supported by previous results; red question marks indicate specific downstream effects to be
958 tested. (B) CgMsn4 nuclear localization in WT and *rim15*∆ strains in -Pi or rich media. Left:
959 CgMsn4-GFP, % of cells with $CgMsn4^{nuc}$ labeled on the lower left; right: bright field (BF) showing
960 cells. Fisher's Exact Tests (FET) were performed to compare the two strains under each condition.
961 Raw, two-sided *P*-values were reported on the side. (C) Cta1-GFP induction during -Pi. Dots are
962 the means of >3 biological replicates and the error bars the 95% CI based on 1000 bootstraps.
963 (D) ASR assay for the wild type (WT) and *rim15*∆. Shown are survival rates of the two strains at
964 an equivalent H_2O_2 strength, either with (-Pi) or without (Mock) a primary stress. Each dot is an
965 independent biological replicate (n = 7) and the red bar represents the mean. Basal survival rates
966 were not different between the two strains (P = 0.5). The ASR effect is significant in both (raw,
967 one-sided P = 0.008 for both), but is significantly lower in *rim15*∆ (mean ASR-score = 6.29 in WT
968 vs 3.45 in *rim15*∆, Mann-Whitney U test, two-sided P = 0.04).
969
970
971 **Figure 7. TORC1 is strongly inhibited by phosphate starvation in *C. glabrata*, likely**
972 **contributing to the ASR via its proximal kinase, Sch9.** (A) A representative Western Blot for
973 phosphorylated Rps6 (P-Rps6) and total Rps6 in both species under rich media, nitrogen

974 starvation (-N) or phosphate starvation (-Pi) conditions. Red arrows point to the loss vs presence
975 of the P-Rps6 band under -Pi in *C. glabrata* and *S. cerevisiae*, respectively. (B) Quantification
976 of %P-Rps6 over total Rps6 (n=3). *Bonferroni corrected *P*-values from Student's t-tests were
977 shown. (C) Inhibiting TORC1 by rapamycin induces Cta1-GFP in a dose-dependent manner. The
978 dots, error bars and lines have the same meaning as before. (D) ASR for H_2O_2 with rapamycin as
979 the primary treatment. Plotted are survival rates with or without rapamycin treatment (n=12 for *C.*
980 *glabrata*, n=8 for *S. cerevisiae*). 60 mM and 6 mM of H_2O_2 were used as the secondary stress for
981 the two species, resulting in a similar basal survival rate (P = 0.6). A Wilcoxon signed-rank test
982 was used to compare the paired experiments with or without the primary treatment for each
983 species. The raw, one-sided *P*-values were shown on the top. (E) Same plot as C, comparing
984 Cta1-GFP induction in a phosphomimetic mutant of Sch9, a key proximal effector of TORC1, and
985 a matching wild type Sch9 strain. (F) Same as D but with phosphate starvation (-Pi) as the primary
986 stress, comparing the Sch9-3E mutant (n=4) and the matching Sch9-wt control (n=4). 100 mM
987 and 40 mM of H_2O_2 were used as the secondary stress for the two genotypes, resulting in a similar
988 basal survival rate (P = 0.7).
989
990 **Figure 8. ASR divergence and rewiring of the underlying regulatory network.** (A) Phosphate
991 starvation elicits a fast and strong induction of oxidative stress response (OSR) genes in *C.*
992 *glabrata* in addition to the canonical phosphate starvation response (right), providing strong
993 acquired resistance for a secondary H_2O_2 challenge; in the related *S. cerevisiae*, the induction of
994 OSR genes is much weaker and slower, explaining its lack of ASR. The orange arrows in the right
995 diagram indicate evolutionary rewiring in part of the response to phosphate limitation between the
996 two species. (B) Evolutionary rewiring at the transcriptional level. Regulation of OSR genes such
997 as *CTA1* involves some of the same transcription factors (TFs) during both oxidative stress and
998 phosphate starvation, but with different combinatorial logic. Width of the arrow indicates the
999 importance of the TF; the wide arrows to the right of the TFs indicate their combinatorial logic.
1000 Asterisks indicate potential evolutionary events, both at the *trans*- and *cis*- (promoter)
1001 levels. Combined, they lead to distinct induction kinetics under the two stimuli (right). (C)
1002 Proposed rewiring in the Target-of-Rapamycin Complex 1 (TORC1). Nitrogen-sensing is
1003 conserved between species and strongly activate two of TORC1's downstream branches. By
1004 contrast, sensing of phosphate is evolutionarily labile; it strongly activates the stress response
1005 branch but very weakly affects the nitrogen catabolism branch. The question mark indicates we
1006 still lack direct evidence for TORC1 being responsible for the stress gene induction in the ASR.
1007 This model suggests that flexibility in connecting individual stimulus with specific downstream
1008 branch(es) allows TORC1 to contribute to the ASR evolution by avoiding pleiotropic effects.
1009

1010 **Tables**

1011 **Table 1. Yeast strains used in this study**

Strain name	ID	Genotype	Source	Figure
C. glabrata BG99	yH181	[BG2] his3Δ(1 + 631)	(Cormack and Falkow 1999)	Fig. 7, S2, S3, S4, S10

C. glabrata BG99 derivative	yH001; yH002	[BG2] ura3::pUC19; his3Δ(1+631)	(He *et al.* 2017)	Fig. 1, 3, 5, 6, 7, S1, S4, S6, S8, S9, S10, S15
S. cerevisiae K699	yH154	[W303] *MATa ade2-1 trp1-1 can 1-100 leu2-3,112 his3-11,15 ura3* GAL+	ATCC #200903	Fig. 1, 6, 7, S1, S2, S10
S. cerevisiae S288C	yH545	[S288C] *MATα his3Δ200 leu2Δ1 ura3-52 trpΔ63 lys2Δ202 canR cyhR*	Gift from Dr. Jan Fassler	Fig. S12, S15
K. lactis	yH149	[NRRL Y-1440] wild type	ATCC #8585	Fig. S10
L. waltii	yH217	[NCYC 2644] wild type	Gift from Dr. Chris Hittinger	Fig. S10
CTA1-GFP	yH298; yH299	[BG99] *cta1::CTA1-GFP*	This study	Fig. 3, 4, 6, 7, S4, S5, S7
MET3pr-CTA1-GFP	yH737	[BG99] *MET3pr::CTA1-GFP*	This study	Fig. S5
cta1Δ	yH271; yH272	[BG99] *cta1::URA3*	This study	Fig. 3, 4, S3, S4, S6
cta1::CTA1	yH285; yH286	[BG99] *cta1::CgCTA1*	This study	Fig. S3, S4, S6
msn2Δ	yH417; yH418; yH419	[BG99] *msn2::HIS3; cta1::CTA1-GFP*	This study	Fig. 4, S7
msn4Δ	yH429; yH430; yH431	[BG99] *msn4::NAT; cta1::CTA1-GFP*	This study	Fig. 4, 6, 7, S7
msn2Δ msn4Δ	yH433; yH434; yH435	[BG99] *msn2::HIS3; msn4::NAT; cta1::CTA1-GFP*	This study	Fig. 4, S7
pho4Δ	yH005	[BG99] *pho4::URA3;*	This study	Fig. S6
rim15Δ	yH609; yH610	[BG99] *rim15::HIS3;*	This study	Fig. 6, S9
rim15Δ CTA1-GFP	yH520; yH521; yH522	[BG99] *rim15::HIS3; cta1::CTA1-GFP*	This study	Fig. 6
rim15::RIM15	yH731; yH732	[BG99] *rim15::RIM15*	This study	Fig. S9

msn4Δ rim15Δ	yH523; yH524; yH525	[BG99] *msn4::NAT; rim15::HIS3; cta1::CTA1-GFP*	This study	Fig. 6
skn7Δ	yH440; yH441; yH442	[BG99] *skn7::HIS3; cta1::CTA1-GFP*	This study	Fig. 4, S7
yap1Δ	yH426	[BG99] *yap1::Nat*	This study	Fig. S6
yap1Δ CTA1-GFP	yH446; yH447; yH449	[BG99] *yap1::HIS3; cta1::CTA1-GFP*	This study	Fig. 4, S7
msn4Δ skn7Δ	yH454; yH455; yH457	[BG99] *msn4::NAT; skn7::HIS3; cta1::CTA1-GFP*	This study	Fig. S7
yap1Δ skn7Δ	yH452; yH453	[BG99] *skn7::NAT; yap1::HIS3; cta1::CTA1-GFP*	This study	Fig. S4
4OL	yH352; yH335; yH336	[BG99] *200bp - 400bp upstream of translational start site of CTA1 removal ; cta1::CTA1-GFP*	This study	Fig. 4
8OL	yH340; yH341; yH342	[BG99] *600bp - 800bp upstream of translational start site of CTA1 removal ; cta1::CTA1-GFP*	This study	Fig. 4
muMsn4BS#1	yH353; yH354; yH355	[BG99] *Msn4 binding site mutation 1; cta1::CTA1-GFP*	This study	Fig. 4
muMsn4BS#2	yH384; yH385; yH386	[BG99] *Msn4 binding site mutation 2; cta1::CTA1-GFP*	This study	Fig. 4
muSkn7BS#1	yH403; yH404	[BG99] *Skn7 binding site mutation 1; cta1::CTA1-GFP*	This study	Fig. 4
muSkn7BS#2	yH405; yH406; yH407	[BG99] *Skn7 binding site mutation 1; cta1::CTA1-GFP*	This study	Fig. 4
ScMsn4-mCitrine ScMsn2-mcherry	yH223	[W303] Nhp6a-iRFP-Kan, Msn4-mCitrine(v163A)-spHIS5 Msn2-mCherry-Trp, *leu::PRS305*	(AkhavanAghdam *et al.* 2016)	Fig. 5, S8

ScDAL80pr-GFP	yH646; yH647; yH648	[BG99] *msn2::ScDal80pr-GFP*	This study	Fig. S12
C. glabrata budding assay	yH654	[BG99] pCU (pgrb2.1) *CgPHO84p::yeGFP*	This study	Fig. S15
S. cerevisiae budding assay	yH677	[S288C] *ura3::PHO84pr-GFP-URA3*	This study	Fig. S15
Sch9-WT-NAT	yH692; yH693; yH694; yH695	[BG99] *sch9::Sch9-WT-NAT; cta1::CTA1-GFP*	This study	Fig. 7
Sch9-3E-NAT	yH699	[BG99] *sch9::Sch9-3E-NAT; cta1::CTA1-GFP*	This study	Fig. 7

1012

1013 **Table 2. Yeast expression plasmids used in this study**

Plasmids	ID	Description	Source	Figure
pCU-PDC1-GFP	pH078	CEN, URA3, yeGFP	PMID:23934995	
CgMsn4-GFP	pH153	pCU-PDC1-CgMsn4-yeGFP	This study	Fig. 5, 6
CgMsn2-GFP	pH152	pCU-PDC1-CgMsn2-yeGFP	This study	Fig. S8
ScDAL80pr-GFP	pH306	pKW431-*ScDAL80pr*-yeGFP	This study	Fig. S12

1014

1015 **Table 3. qRT-PCR Primers used in this study**

Primer Description	ID	Sequence (5’ to 3’)	Source	Figure
CgCTA1 reverse qPCR primer	oH423	5’- CTGTCTTGGTTTGGAATTTGGTA -3’	This study	Fig. 3
CgCTA1 forward qPCR primer	oH424	5’ - ATCCCTGTCAACTGCCCATAC - 3’	This study	Fig. 3
CgCTA1 reverse qPCR primer	oH1347	5’- CCACTTTCGTCGTATTCTTGCTTG - 3’	This study	Fig. 3
CgACT1 forward qPCR primer	oH1348	5’- GACCAAACTACTTACAACTCC -3’	This study	Fig. 3

1016

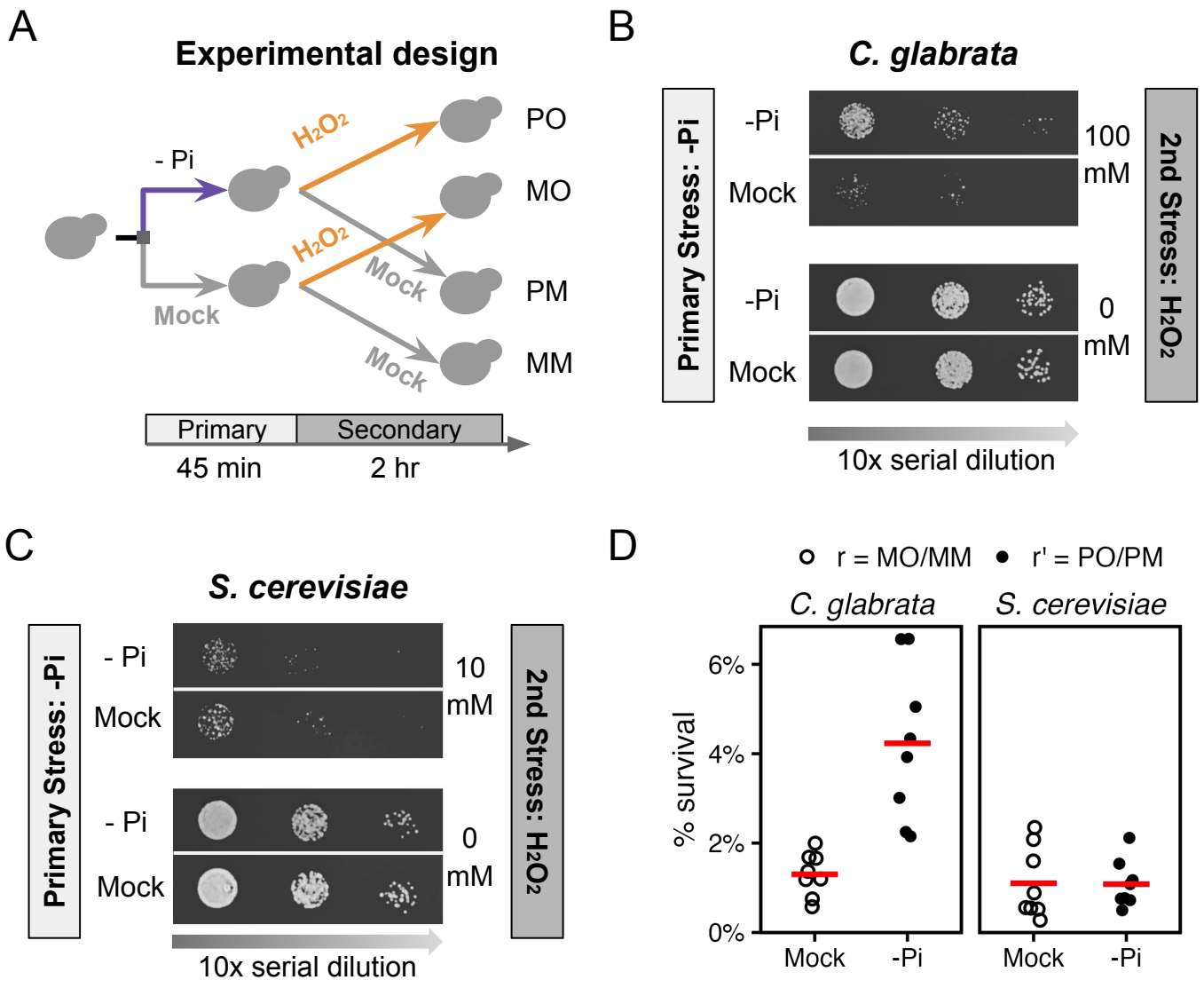

Figure 1. Phosphate starvation induces strong acquired resistance for H_2O_2 in *C. glabrata* and not in *S. cerevisiae*. (A) Experimental design for quantifying Acquired Stress Resistance (ASR): cells were first treated with phosphate starvation (-Pi, or P) or mock-treated (M), then exposed to a secondary H_2O_2 (O) stress or a mock treatment (M). The resulting treatment regimens were referred to as PO, MO, PM and MM. After each treatment regimen, *C. glabrata* (B) and *S. cerevisiae* (C) cells were spotted on rich solid media and imaged after 24-48 hrs. Different H_2O_2 concentrations were used for the two species to achieve a similar survival rate without the primary stress. (D) Survival rates (%) after the secondary H_2O_2 challenge were quantified using Colony Forming Units either with (r') or without (r) phosphate starvation as a primary stress. The biological replicates (n=8) were shown as dots and their means as bars. Basal survival rates (r) were not different between species (P = 0.38), while there was a significant increase in survival due to the primary stress in *C. glabrata* but not in *S. cerevisiae* (raw P-values = 0.0039 and 0.37, respectively).

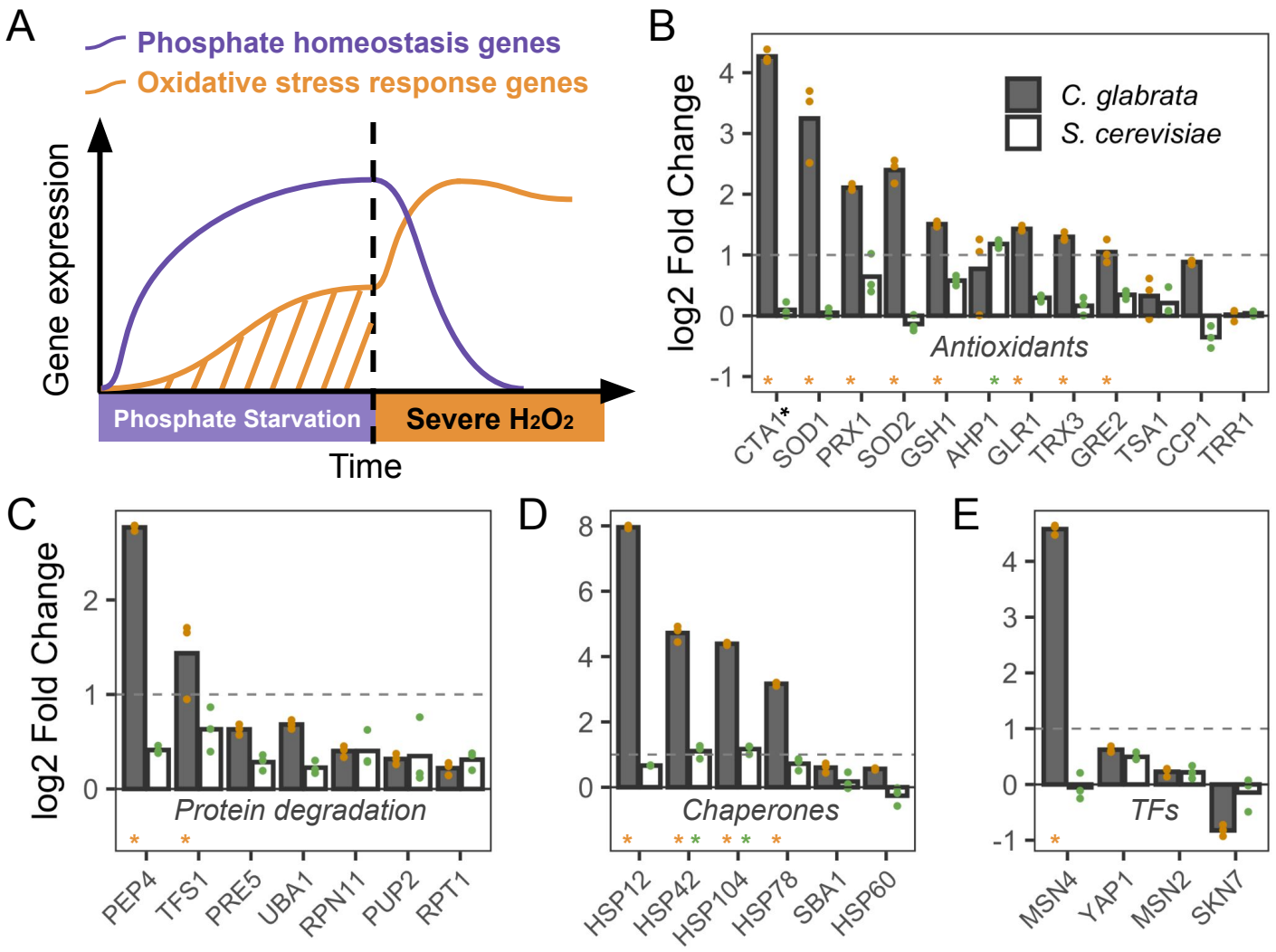

Figure 2. Phosphate starvation strongly induces many oxidative stress related genes in *C. glabrata* but not in *S. cerevisiae*. (A) Proposed transcriptional basis for the acquired stress resistance in *C. glabrata*: phosphate starvation induces both canonical phosphate homeostasis genes and also oxidative stress response genes, providing protection for the secondary H_2O_2 challenge. (B-E) Comparison of transcriptional induction of genes known to be involved in OSR in *S. cerevisiae*. Log2 fold changes after 1 hour of phosphate starvation were shown as the mean (bar) of 3 biological replicates (dots) for genes encoding antioxidants (B), protease components (C), molecular chaperones (D) and TFs involved in the OSR (E). The dotted lines indicate a 2 fold induction. Gene names were based on *S. cerevisiae* except for *CTA1*, which had two paralogs in *S. cerevisiae* and only one in *C. glabrata*. *S. cerevisiae CTT1* is involved in OSR and its fold change is shown in (B). Asterisks above a gene name indicate that the gene was significantly induced in that species at an FDR of 0.05.

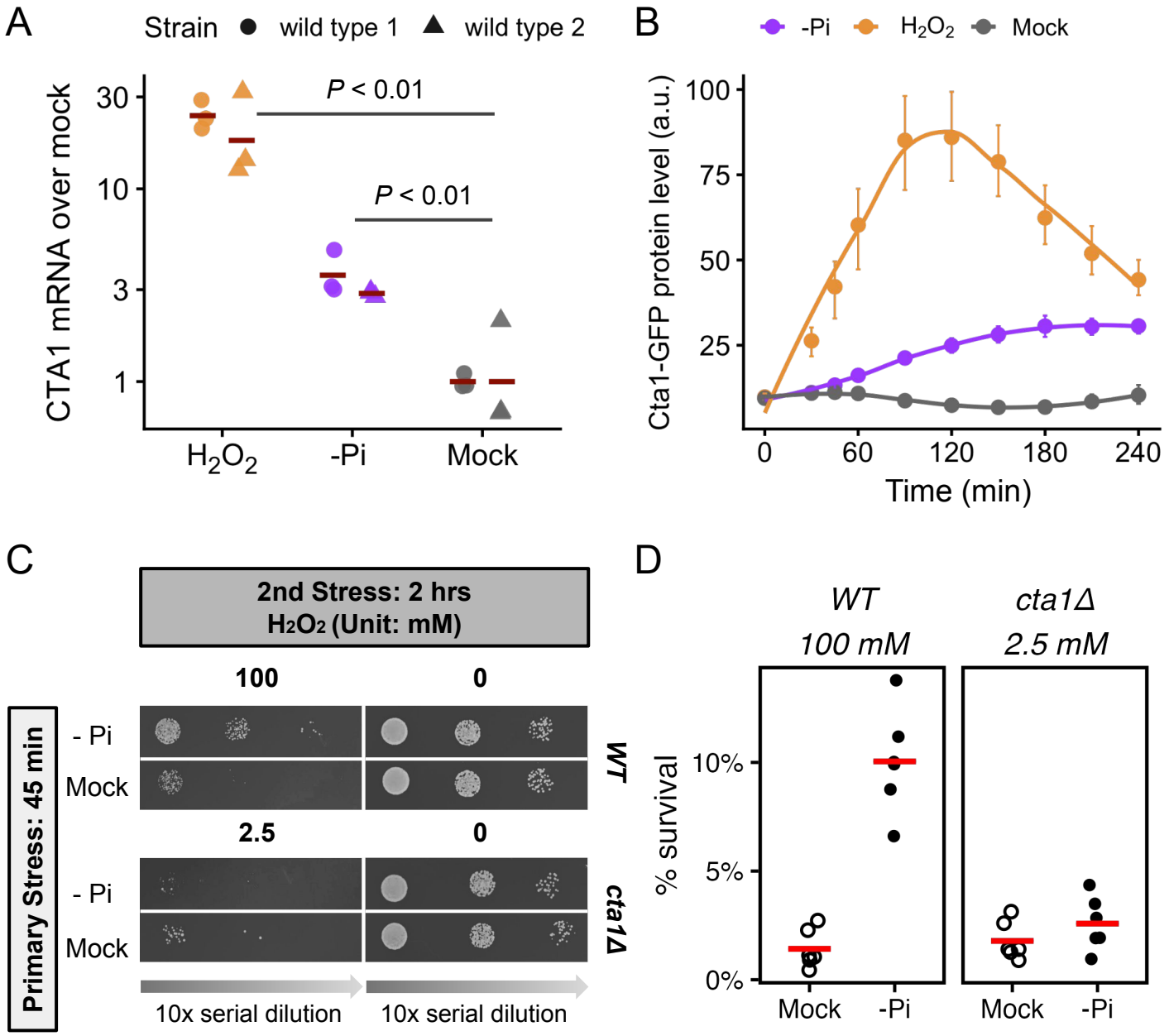

Figure 3. *C. glabrata CTA1* is induced during phosphate starvation and is required for the acquired resistance to severe H_2O_2 stress. (A) *CTA1* mRNA levels were assayed using qRT-PCR following 45 minutes of either 1.5 mM H_2O_2, phosphate starvation or mock treatment. Fold changes over the mock treated samples were shown using *ACT1* as a reference. Two isogenic lab strains of *C. glabrata* were each assayed in triplicates. Bars represent the mean of each strain. An unpaired Student's t-test comparing the $\Delta\Delta C_T$ values between both treatments with the mock found both to be significantly elevated ($P < 0.01$, strain was included as a covariate and found to be not significant). (B) Cta1 protein levels were monitored in strains carrying a genomic *CTA*1-GFP fusion using flow cytometry for 4 hours, during which cells were exposed to either mild H_2O_2 stress, phosphate starvation or mock treatment. The y-axis values are the median fluorescence intensities (a.u. = arbitrary unit). The dots show the mean of >3 biological replicates; the error bars show 95% confidence intervals based on bootstrapping and the lines are LOESS curves fitted to the data. (C) ASR spotting assays for wild type and *cta1*Δ *C. glabrata* strains. 2.5 mM H_2O_2 was used as the secondary stress for *cta1*Δ, which resulted in a similar basal survival rate as 100 mM H_2O_2 for the wild type. (D) ASR effects were quantified by comparing the survival rates after H_2O_2 treatments either with (solid circles) or without (open circles) phosphate starvation. Each dot is an independent experiment (n = 6). The difference in basal survival rates was not statistically significant between the wild type and the *cta1*Δ strain ($P = 0.39$). Phosphate starvation significantly increased the survival of both strains during the secondary challenge (raw $P = 0.016$ in both), but the ASR effect size was much smaller in *cta1*Δ (mean ASR-scores = 9.8 and 1.5 in wild type and *cta1*Δ, respectively; Mann-Whitney U test two-sided $P = 0.001$).

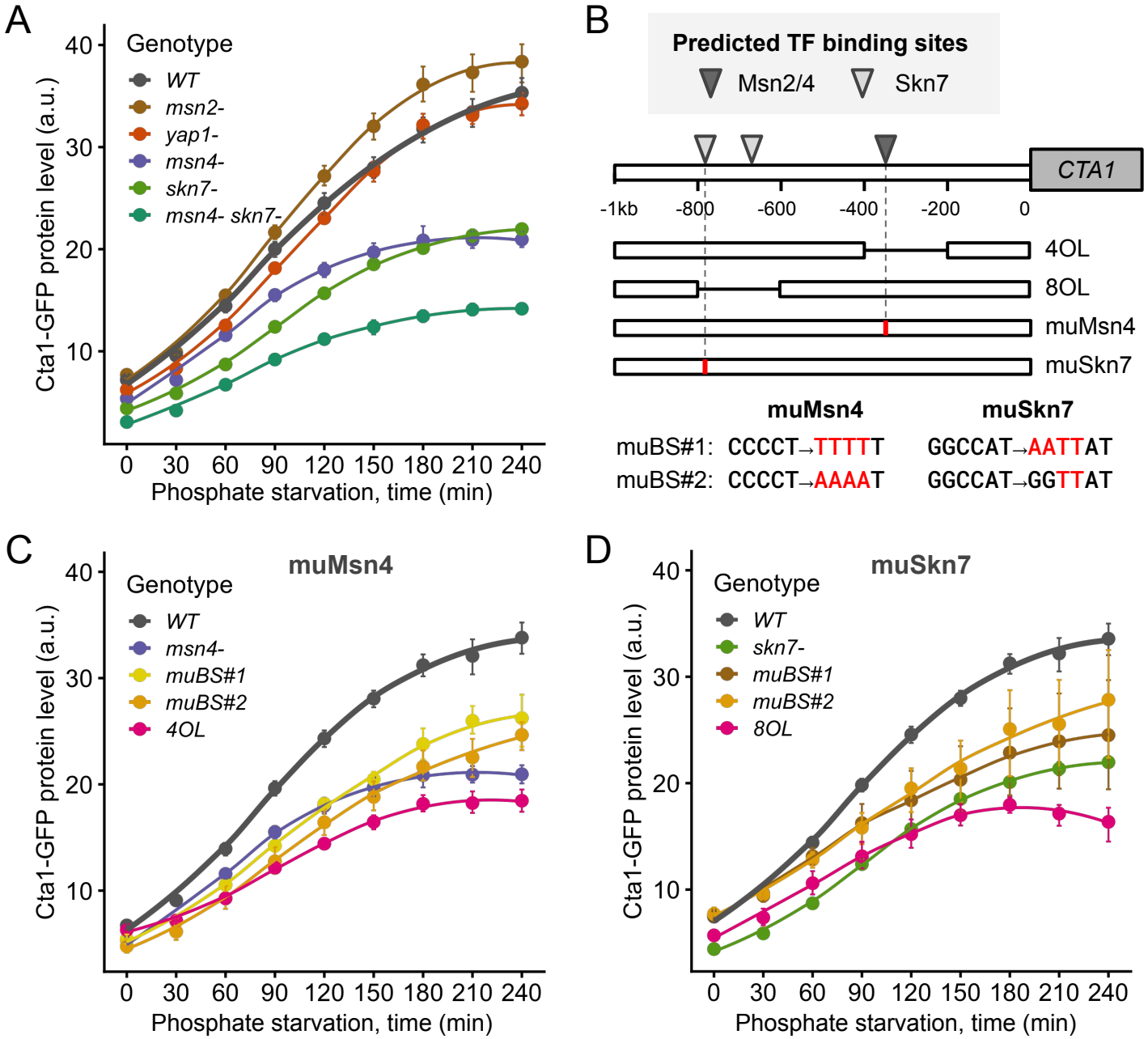

Figure 4. TFs CgMsn4 and CgSkn7 jointly contribute to *CTA1* induction during phosphate starvation in *C. glabrata*. (A) Cta1-GFP levels over 4 hours of phosphate starvation for wild type (WT) and TF deletion mutants. The dots represent the mean of >3 biological replicates and the error bars the 95% confidence interval based on 1000 bootstrap replicates. The lines are LOESS fit to the data. (B) A schematic showing the predicted binding sites (BS) for Skn7 and Msn2/Msn4 in *C. glabrata* (Materials and Methods). Based on the prediction, two types of *cis*-mutants were created: the internal deletions (4OL, 8OL) each removed 200 bp containing either the predicted Msn2/Msn4 BS or both Skn7 BS; four point mutation alleles each targeted either the single Msn2/Msn4 BS or one of the Skn7 BS predicted to have a higher affinity. (C, D) Comparing the Cta1-GFP induction driven by each of the mutant promoters in (B) compared with the WT and the corresponding TFΔ mutant.

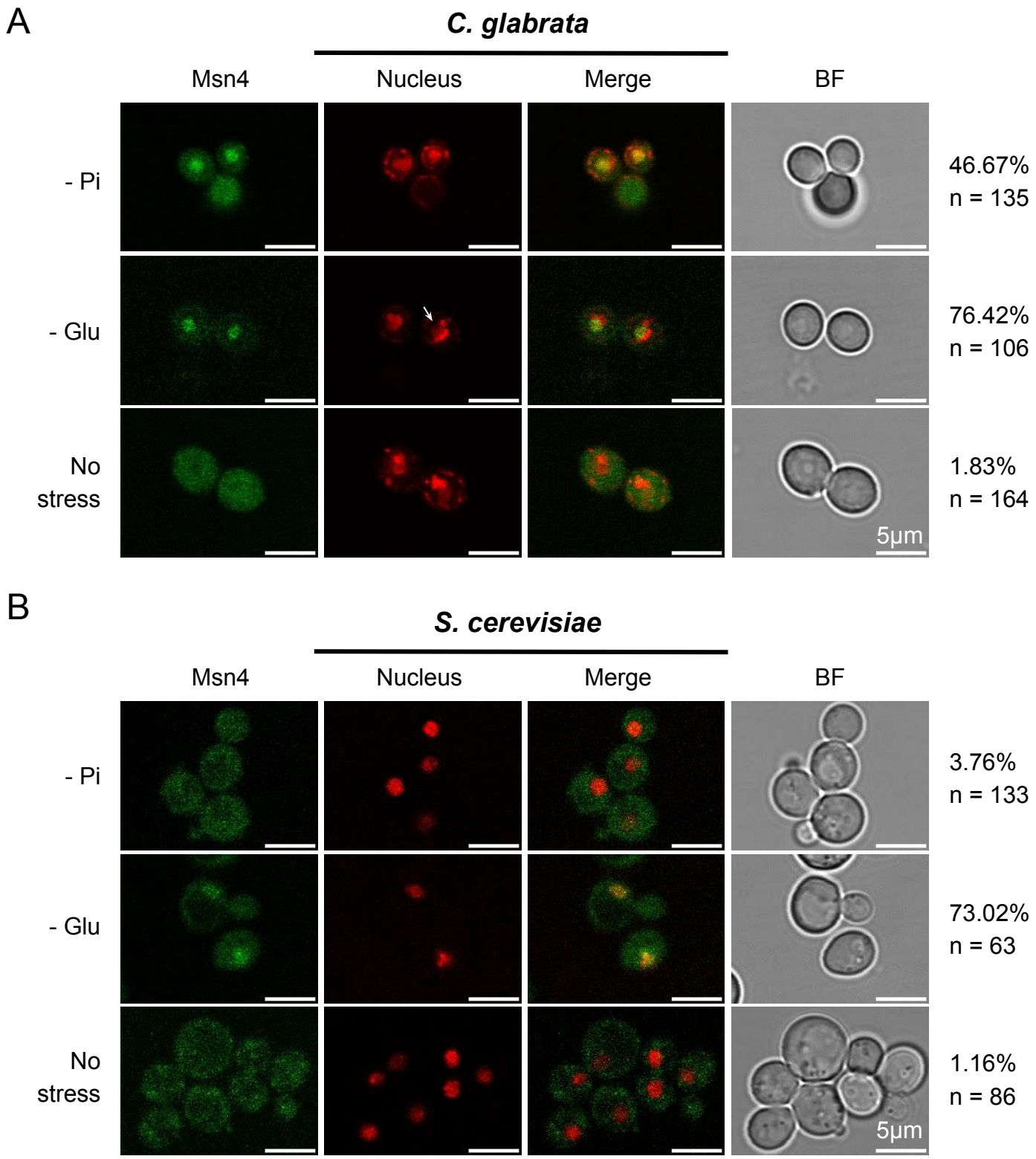

Figure 5. *C. glabrata* Msn4 (CgMsn4) translocates into the nucleus upon phosphate starvation but not its ortholog in *S. cerevisiae* (ScMsn4). Cellular localization of CgMsn4 (A) and ScMsn4 (B) under phosphate starvation (0 mM, -Pi), glucose starvation (0.02% glucose, -Glu), and no stress conditions. All treatments were for 45 minutes. From left to right: i. CgMsn4-yeGFP and ScMsn4-mCitrine; ii. nucleus staining with DAPI in *C. glabrata* or labeled with Nh6a-iRFP in *S. cerevisiae*; iii. merge; iv. bright field. The percent of cells with nuclear-localized Msn4 and the total number of cells examined by microscopy were shown on the right. Scale bars are 5 μm in length.

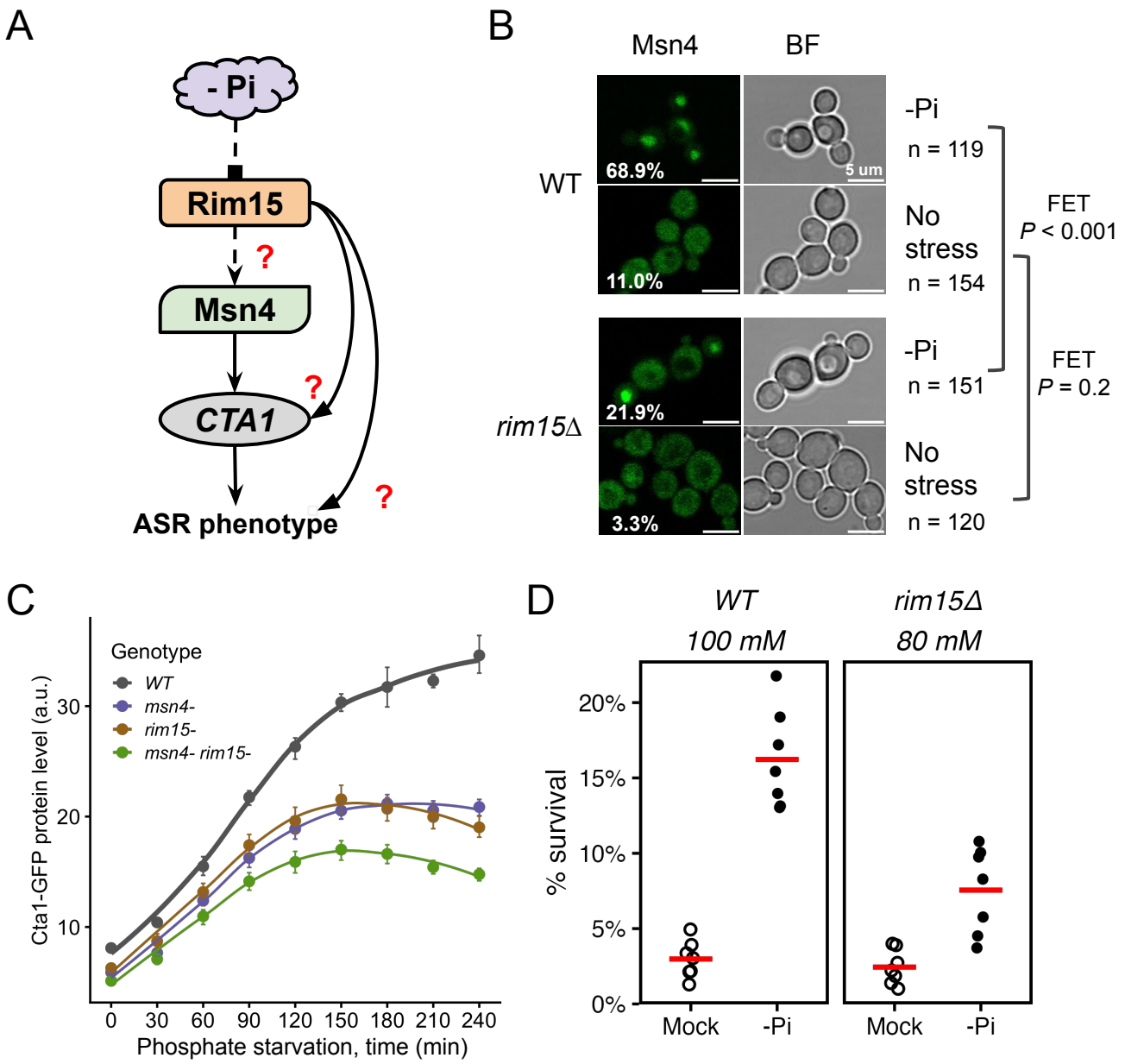

Figure 6. The Greatwall kinase homolog Rim15 mediates phosphate starvation-induced ASR in *C. glabrata*. (A) Proposed model for phosphate starvation-induced ASR in *C. glabrata*: phosphate starvation (-Pi) activates Rim15, which goes on to regulate Msn4's activity and contributes to ASR. Dashed arrows show proposed connections; solid arrows are regulations supported by previous results; red question marks indicate specific downstream effects to be tested. (B) CgMsn4 nuclear localization in WT and *rim15*Δ strains in -Pi or rich media. Left: CgMsn4-GFP, % of cells with CgMsn4^{nuc} labeled on the lower left; right: bright field (BF) showing cells. Fisher's Exact Tests (FET) were performed to compare the two strains under each condition. Raw, two-sided *P*-values were reported on the side. (C) Cta1-GFP induction during -Pi. Dots are the means of >3 biological replicates and the error bars the 95% CI based on 1000 bootstraps. (D) ASR assay for the wild type (WT) and *rim15*Δ. Shown are survival rates of the two strains at an equivalent H_2O_2 strength, either with (-Pi) or without (Mock) a primary stress. Each dot is an independent biological replicate (n = 7) and the red bar represents the mean. Basal survival rates were not different between the two strains (P = 0.5). The ASR effect is significant in both (raw, one-sided P = 0.008 for both), but is significantly lower in *rim15*Δ (mean ASR-score = 6.29 in WT vs 3.45 in *rim15*Δ, Mann-Whitney U test, two-sided P = 0.04).

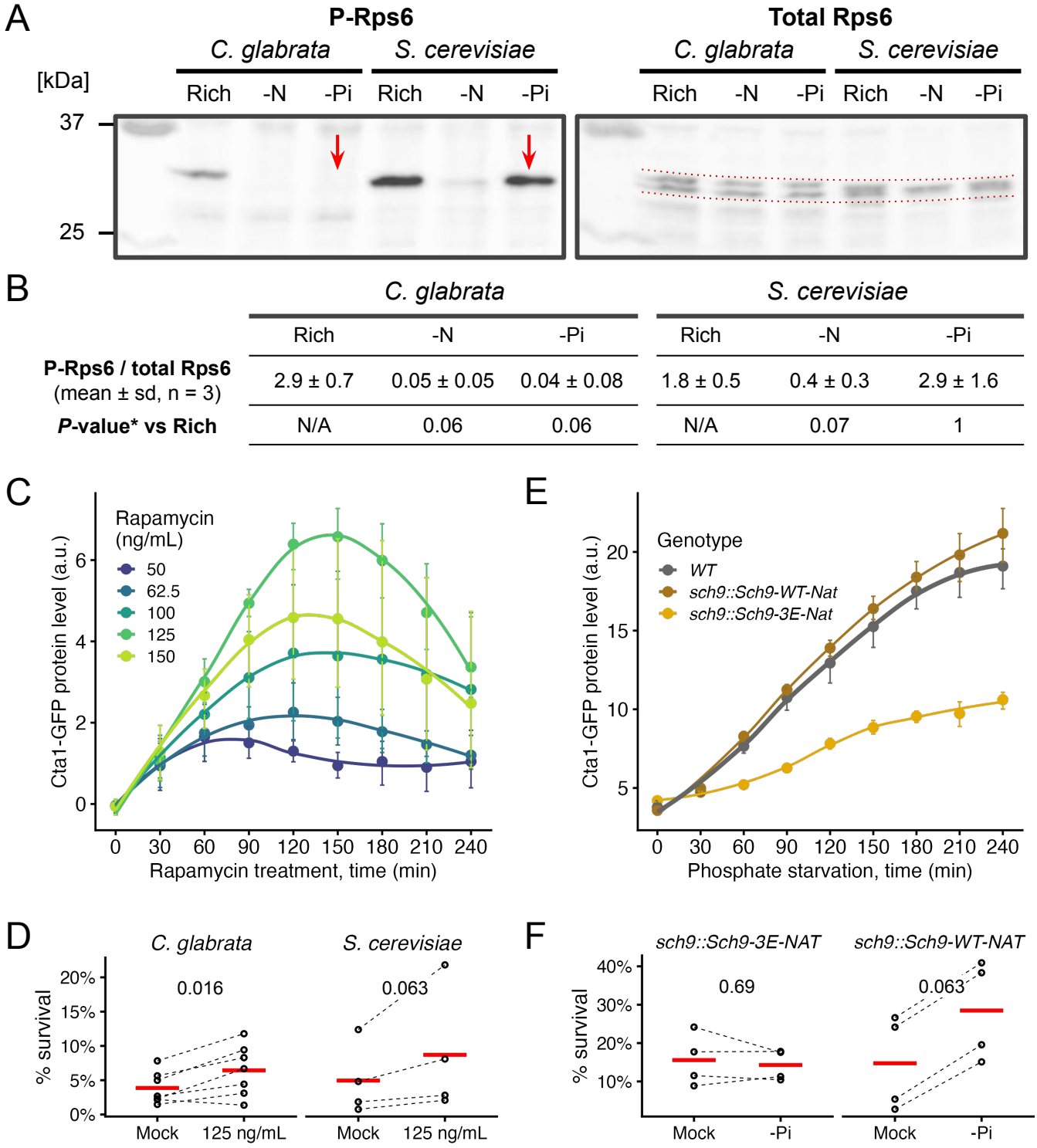

Figure 7. TORC1 is strongly inhibited by phosphate starvation in *C. glabrata*, likely contributing to the ASR via its proximal kinase, Sch9. see after Figure 8 for legends.

Figure 7. TORC1 is strongly inhibited by phosphate starvation in *C. glabrata*, likely contributing to the ASR via its proximal kinase, Sch9. (A) A representative Western Blot image for phosphorylated Rps6 (P-Rps6) and total Rps6 in both species under rich media, nitrogen starvation (-N) or phosphate starvation (-Pi) conditions. Red arrows point to the loss vs presence of the P-Rps6 band under -Pi in *C. glabrata* and *S. cerevisiae*, respectively. The two dotted lines on the right image indicate the regions used for quantifying the total Rps6 amount. (B) Quantification of P-Rps6 / total Rps6 (n=3). *Bonferroni corrected *P*-values from Student's t-tests were shown. (C) Inhibiting TORC1 by rapamycin induces Cta1-GFP in a dose-dependent manner. The dots, error bars and lines have the same meaning as before. (D) ASR for H_2O_2 with rapamycin as the primary treatment. Plotted are survival rates with or without rapamycin treatment (n=12 for *C. glabrata*, n=8 for *S. cerevisiae*). 60 mM and 6 mM of H_2O_2 were used as the secondary stress for the two species, resulting in a similar basal survival rate (P = 0.6). A Wilcoxon signed-rank test was used to compare the paired experiments with or without the primary treatment for each species. The raw one-sided *P*-values were shown on the top. (E) Same plot as C, comparing Cta1-GFP induction in a phosphomimetic mutant of Sch9, a key proximal effector of TORC1, and a matching wild type Sch9 strain. (F) Same as D but with phosphate starvation (-Pi) as the primary stress, comparing the Sch9-3E mutant (n=4) and the matching Sch9-WT control (n=4). 100 mM and 40 mM of H_2O_2 were used as the secondary stress for the two genotypes, resulting in a similar basal survival rate (P = 0.7).

Figure 8. ASR divergence and rewiring of the underlying regulatory network. (A) Phosphate starvation elicits a fast and strong induction of oxidative stress response (OSR) genes in *C. glabrata* in addition to the canonical phosphate starvation response (right), providing strong acquired resistance for a secondary H_2O_2 challenge; in the related *S. cerevisiae*, the induction of OSR genes is much weaker and slower, explaining its lack of ASR. The orange arrows in the right diagram indicate evolutionary rewiring in part of the response to phosphate limitation between the two species. (B) Evolutionary rewiring at the transcriptional level. Regulation of OSR genes such as *CTA1* involves some of the same transcription factors (TFs) during both oxidative stress and phosphate starvation, but with different combinatorial logic. Width of the arrow indicates the importance of the TF; the wide arrows to the right of the TFs indicate their combinatorial logic. Asterisks indicate potential evolutionary events, both at the *trans*- and *cis*- (promoter) levels. Combined, they lead to distinct induction kinetics under the two stimuli (right). (C) Proposed rewiring in the Target-of-Rapamycin Complex 1 (TORC1). Nitrogen-sensing is conserved between species and strongly activate two of TORC1's downstream branches. By contrast, sensing of phosphate is evolutionarily labile; it strongly activates the stress response branch but very weakly affects the nitrogen catabolism branch. The question mark indicates we still lack direct evidence for TORC1 being responsible for the stress gene induction in the ASR. This model suggests that flexibility in connecting individual stimulus with specific downstream branch(es) allows TORC1 to contribute to the ASR evolution by avoiding potential pleiotropic effects.

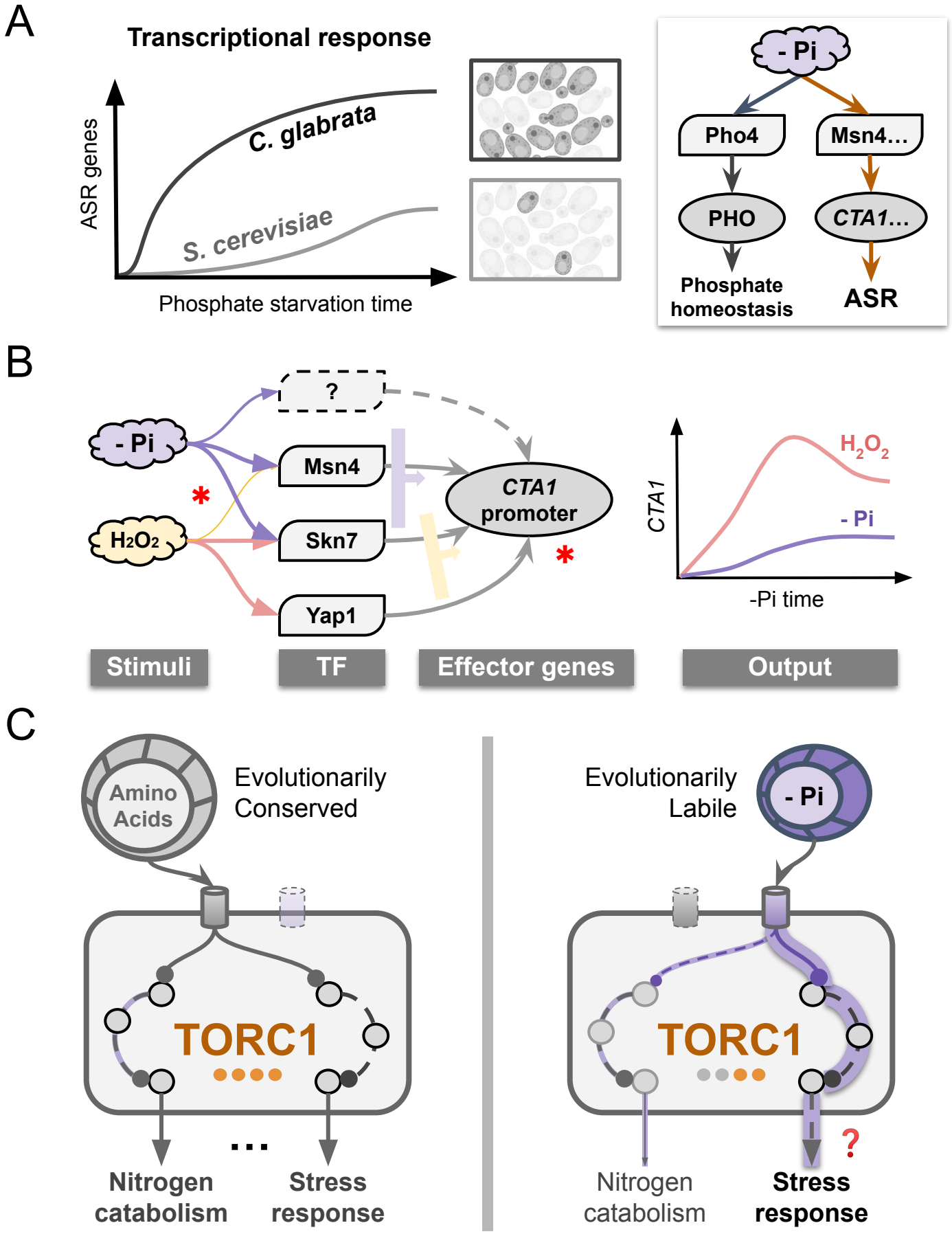

Figure 8. ASR divergence and rewiring of the underlying regulatory network. See next page for legend

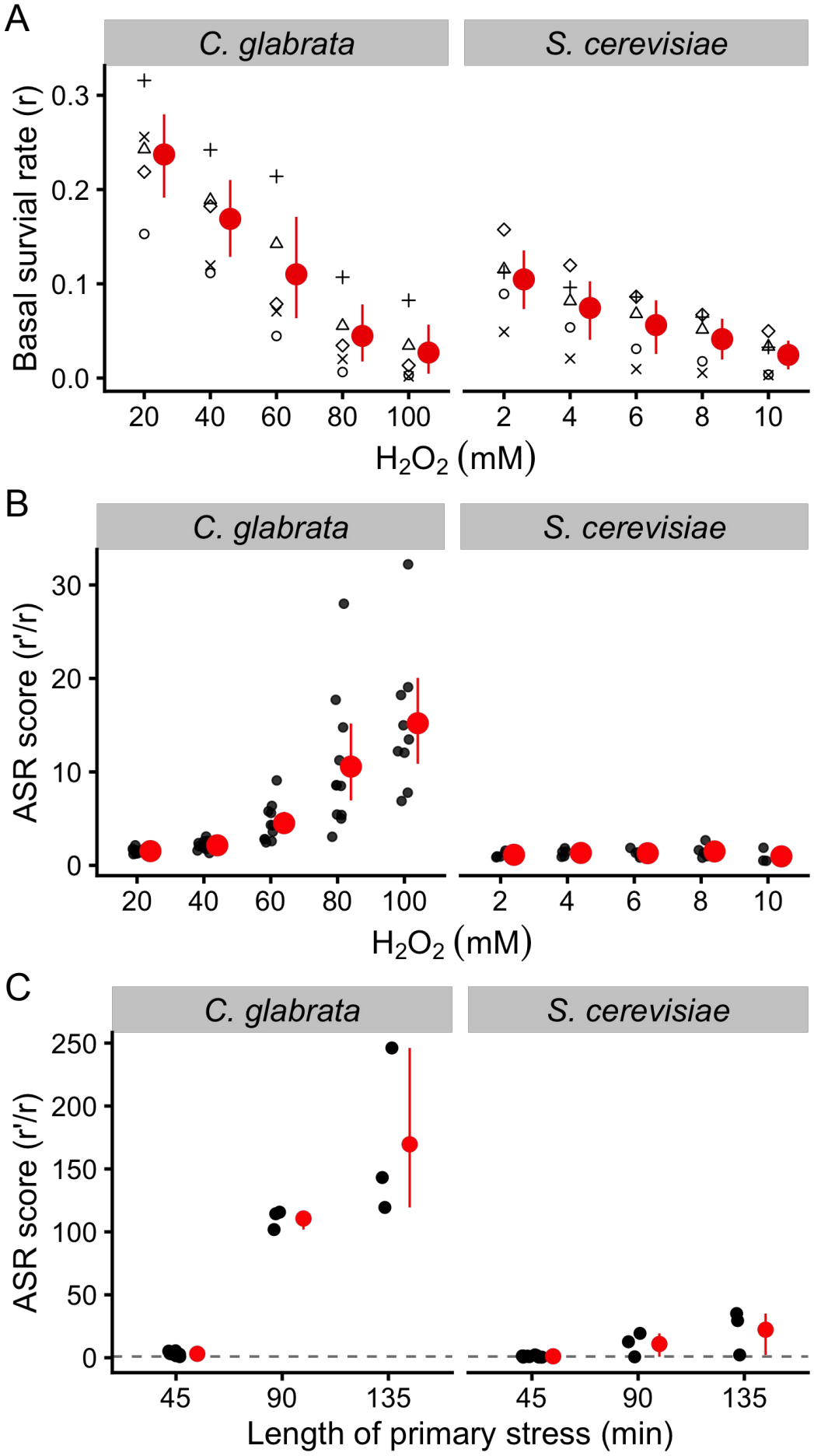
A
C. glabrata
S. cerevisiae
Basal survial rate (r)
0.3
0.2
0.1
0.0
20
40
60
80
100
2
4
6
8
10
H2O2 (mM)
B
C. glabrata
S. cerevisiae
ASR score (r'/r)
30
20
10
0
20
40
60
80
100
2
4
6
8
10
H2O2 (mM)
C
C. glabrata
S. cerevisiae
ASR score (r'/r)
250
200
150
100
50
0
45
90
135
45
90
135
Length of primary stress (min)

Supplementary Figure 1. Basal survival rates and phosphate starvation induced acquired resistance for H_2O_2 at different primary and secondary stress conditions. (A) Basal survival rates (r) at different H_2O_2 concentrations in *C. glabrata* and *S. cerevisiae* were quantified using Colony Forming Unit (CFU) ratios between cells treated with H_2O_2 and mock treated ones. The red dots and vertical lines show the mean and 95% confidence intervals based on 1000 bootstrap replicates. Individual data points are shown in different shapes grouped by the date of the experiment. (B) Acquired Stress Resistance (ASR) at different H_2O_2 secondary stress levels in the two species. ASR-score is defined as the fold increase in survival after the H_2O_2 treatment as a result of the primary stress (phosphate starvation). r' is the survival rate with the primary stress and r is the same as in (A), i.e., without the primary stress. The red dots and lines have the same meanings as in (A). (C) ASR for H_2O_2 at different primary stress length. 100 mM and 10 mM of H_2O_2 were used as the secondary stress for the two species as in Fig. 1. The dotted line shows an ASR score of 1 (i.e., no increase in survival due to the primary stress). A paired t-test was performed on the underlying survival rates (r and r') for each of the six species-by-duration combinations. After Bonferroni correction, all three tests in *C. glabrata* had $P < 0.05$, while all three tests in *S. cerevisiae* yielded $P > 0.5$

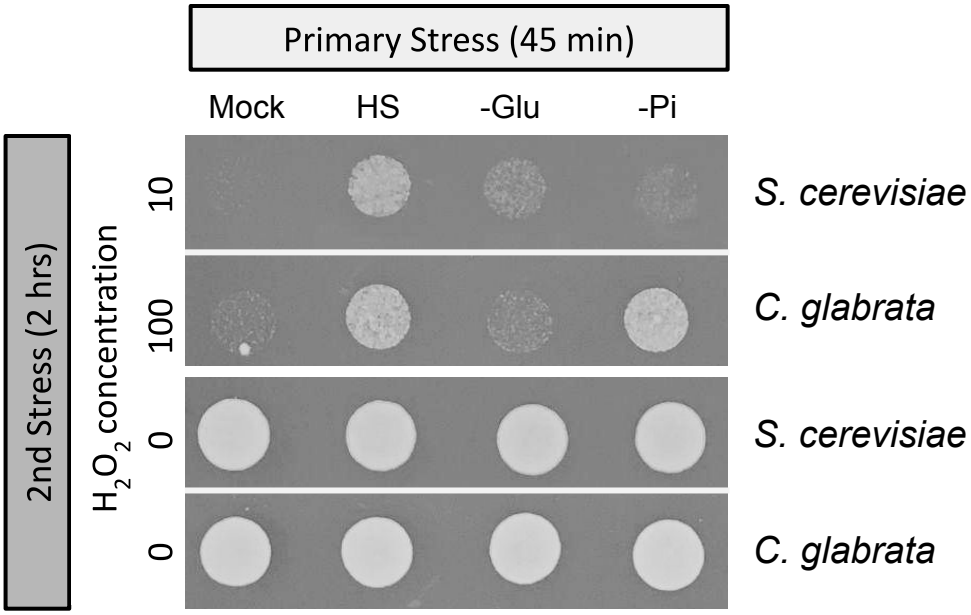

Supplementary Figure 2. Phosphate starvation-induced ASR for H_2O_2 diverge between species while other primary stresses show similar effects. ASR experiment was performed as in Figure 1, with the exception of using different primary stresses as indicated on the top: Mock - rich SC medium; HS - Heat shock at 43C; -Glu - 0.05% glucose (as opposed to 2% in SC); -Pi - no phosphate SC medium. Images were taken 14 hrs and 21 hrs post spotting for *C. glabrata* and *S. cerevisiae* respectively.

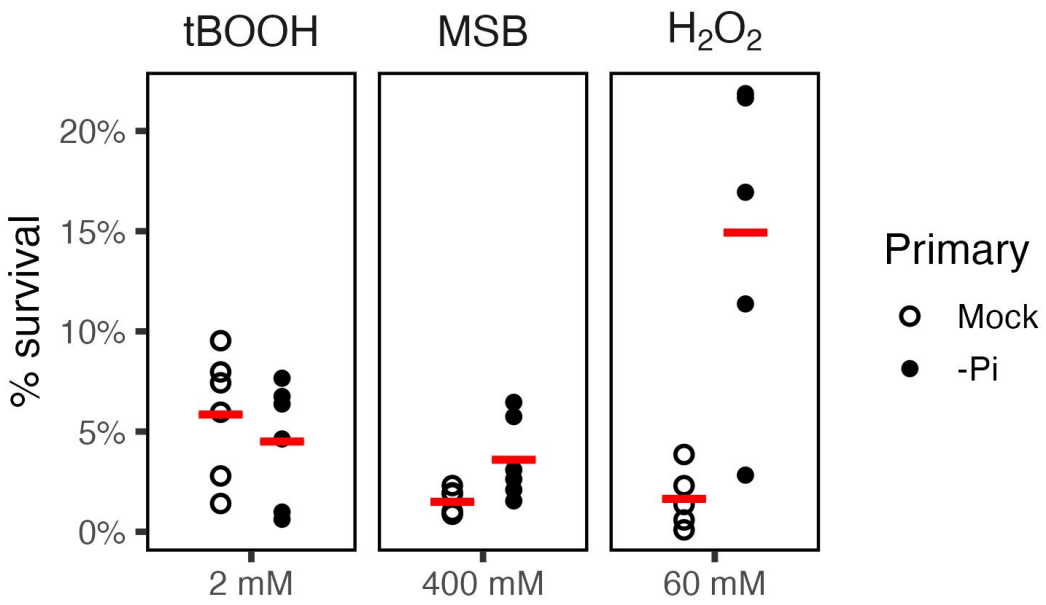

Supplementary Figure 3. Phosphate starvation's ASR effect depends on the type of ROS. We tested the ability of phosphate starvation to provide acquired resistance for two additional ROS, i.e., tert-butyl hydroperoxide and menadione sodium bisulfate (MSB), and compared them to H_2O_2, each at the indicated concentration. No ASR effect was observed for tBOOH (mean ASR-score = 0.71, 95% CI [0.49, 0.88], P = 1). There is moderate ASR for MSB (mean ASR-score = 2.41, 95% CI [1.79, 3.00], raw P = 0.016). ASR for H_2O_2 is the strongest (mean ASR-score = 16.4, 95% CI [7.7, 25.3], raw P = 0.031).

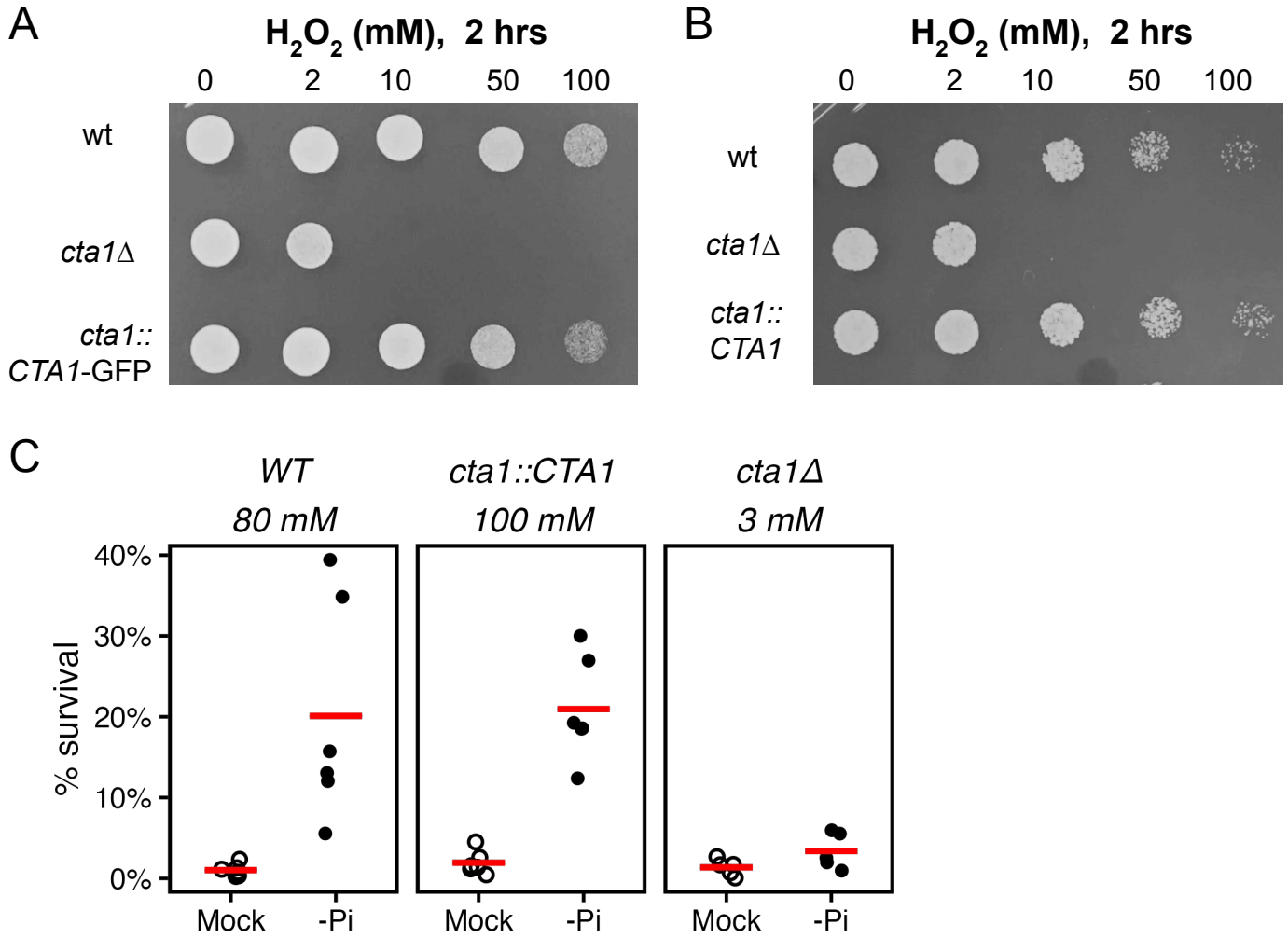

Supplementary Figure 4. *CTA1* complement strain rescues basal H_2O_2 survival and ASR defects in *cta1*Δ. Putting either *CTA1*-GFP (A) or the untagged *CTA1* (B) back to the endogenous locus in the *cta1*Δ background restored the resistance to H_2O_2 compared with the wild type strain. Each strain was treated at the indicated concentrations of H_2O_2 for 2 hours, then spotted onto YPD plates and incubated at 30°C for 48 hours (A) and 20hrs (B). (C) ASR in the wild type, *CTA1* complement (*cta1::CTA1*) and *cta1*Δ strains. The experiment was conducted similarly as in Fig. 3 for wild type and *cta1*Δ strains. Concentrations of H_2O_2 were calibrated to achieve a similar basal survival rates (open circles, Kruskal-Wallis rank sum test for differences among the three groups P = 0.38). ASR-scores for the three strains are (with 95% CI and Wilcoxon signed-rank test P-values in the parenthesis): wild type 23.9 ([14.9, 36.5], P=0.048); *cta1::CTA1* 15.4 ([9.5, 21.3], P=0.048); *cta1*Δ 5.1 ([2.0, 10.6], P=0.093). The difference in ASR-score is significant between *cta1*Δ and wild type, but not between *cta1::CTA1* and wild type (Mann-Whitney U test P = 0.034 and 0.48, respectively, Bonferroni-corrected).

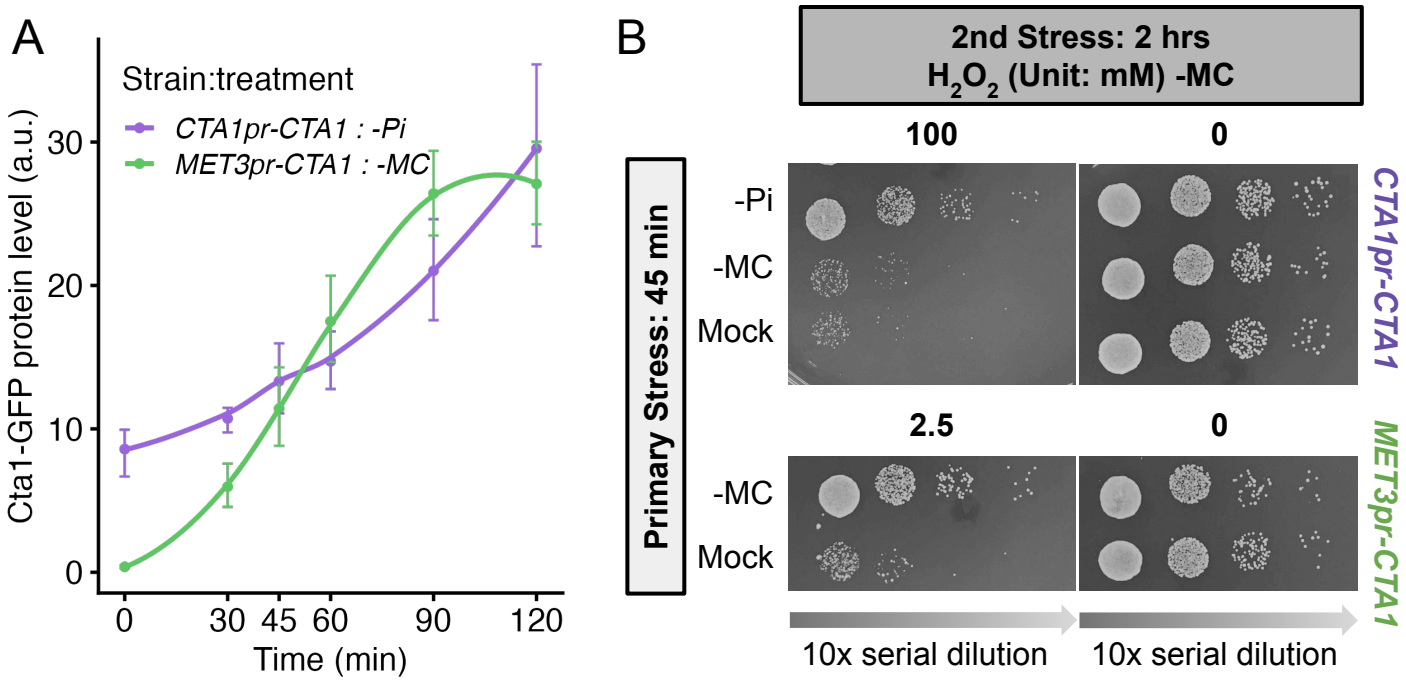

C

Primary stress (45 min)	Secondary Stress (2 hrs)
-Pi : SC w/o Pi	Oxidative: H_2O_2 added to -MC medium
-MC: SC w/o methionine and cysteine	Mock: SC medium
Mock: SC medium	

Supplementary Figure 5. Induction of *CTA1* provides acquired resistance to H_2O_2 in *C. glabrata*. To test if pre-inducing *CTA1* is sufficient to provide ASR for H_2O_2, we replaced the endogenous *CTA1* promoter with the promoter of the *C. glabrata MET3* gene. When grown in SC medium lacking methionine and cysteine (-MC), *CTA1* was induced to a comparable level as in the endogenous *CTA1pr-CTA1* strain under phosphate starvation at 45 minutes (A). Dots represent the mean of at least 3 biological replicates, and the error bars the 95% confidence interval by bootstrapping. The line is the LOESS fit to the data. The endogenous *CTA1pr-CTA1* has a basal expression level that is higher than the *MET3pr-CTA1* (0 min). We also confirmed that the -MC media itself did not provide ASR in the wild type *C. glabrata* cells (B, top). Note that in this set of ASR experiments, all SC medium containing H_2O_2 also lacked methionine and cysteine (C). This allows the *MET3pr-CTA1* to be induced during the secondary stress, mimicking what the wild type strain experiences during the H_2O_2 stress. Using this strain, we found that inducing *CTA1* during the primary stress significantly enhanced the survival of *C. glabrata* cells during the secondary oxidative stress, i.e., providing ASR (B, bottom two rows, -MC vs Mock).

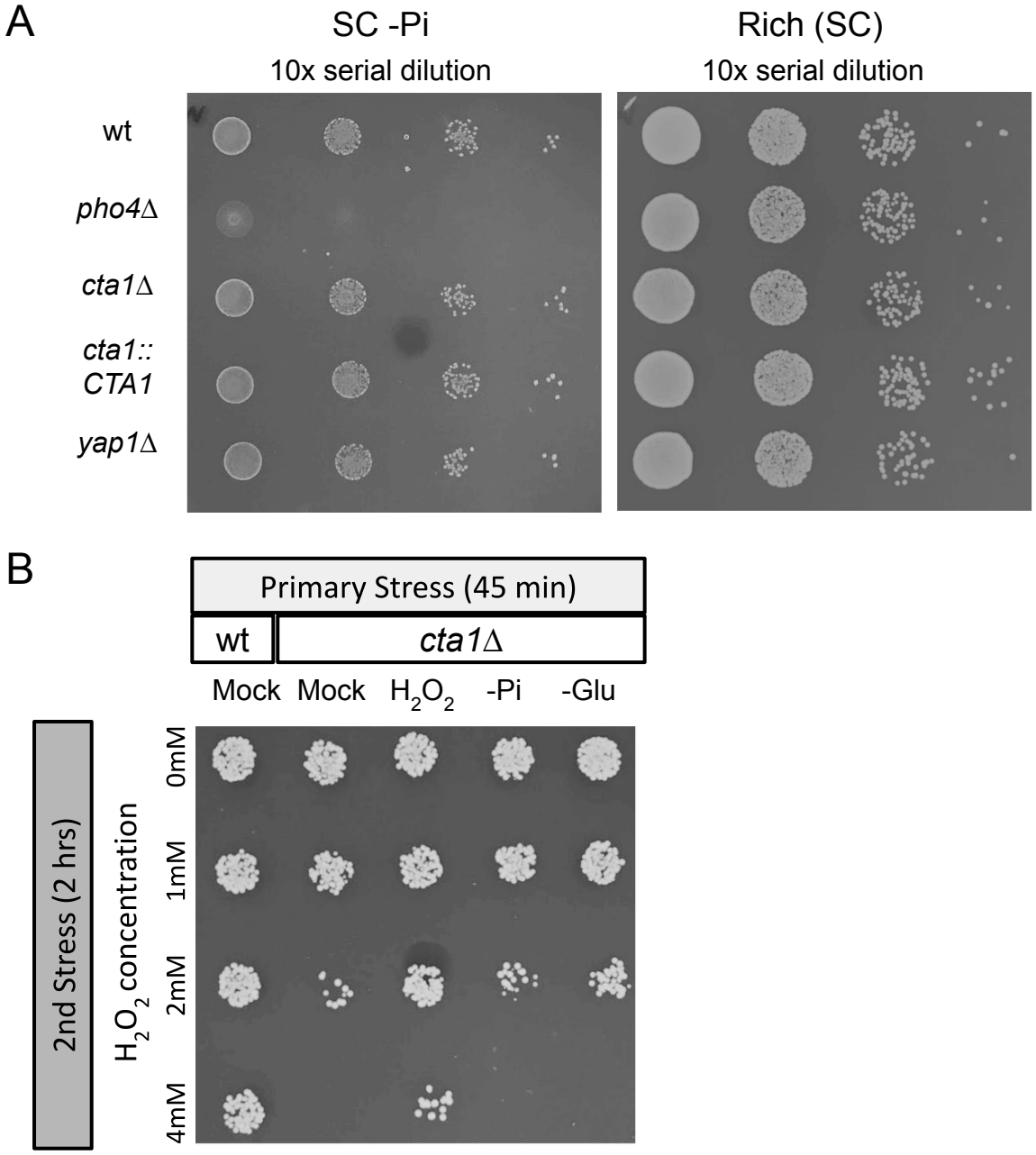

Supplementary Figure 6. Cta1 is not required for survival during the primary phosphate starvation, and is not as important for ASR with mild H_2O_2 used as the primary stress. (A) (Left) Deleting *cta1* and the OSR TF, *yap1*, had no defect on survival under phosphate starvation, while deletion of *pho4*, which is responsible for the PHO response, showed severe growth defects. Mid-log phase cells of the indicated genotypes were spotted on no phosphate SC plates, incubated at 30°C for 48 hours. (Right) Same as (Left) but spotted onto SC plates with 7.5 mM Pi. All images are representatives of >3 biological replicates. (B) *CTA1*'s importance for ASR is dependent on the primary stress type. ASR for wild type and *cta1*Δ were tested with various primary stresses, including phosphate starvation (-Pi), glucose starvation (-Glu, 0.02% glucose), mild H_2O_2 (1.5 mM H_2O_2). ASR experiment was performed as described in the text.

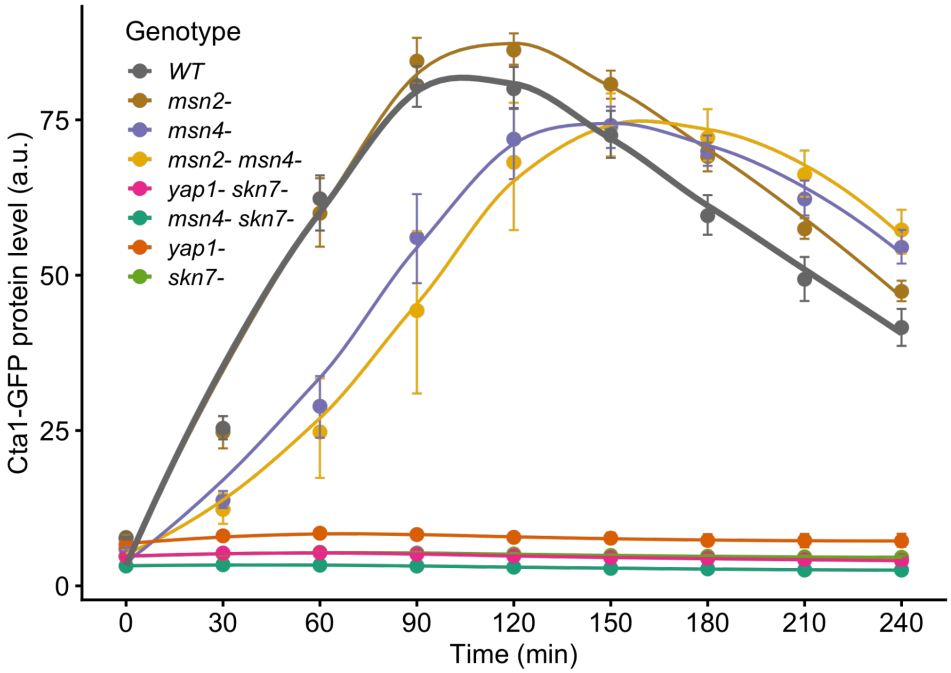

Supplementary Figure 7. TFΔ effects on Cta1-GFP induction under H_2O_2 stress. Cta1-GFP induction under 2 mM H_2O_2 for 4 hours. Yap1, Skn7 play a critical role; Msn4 has a minor contribution while Msn2 is not important. Same features as in Figure 4A.

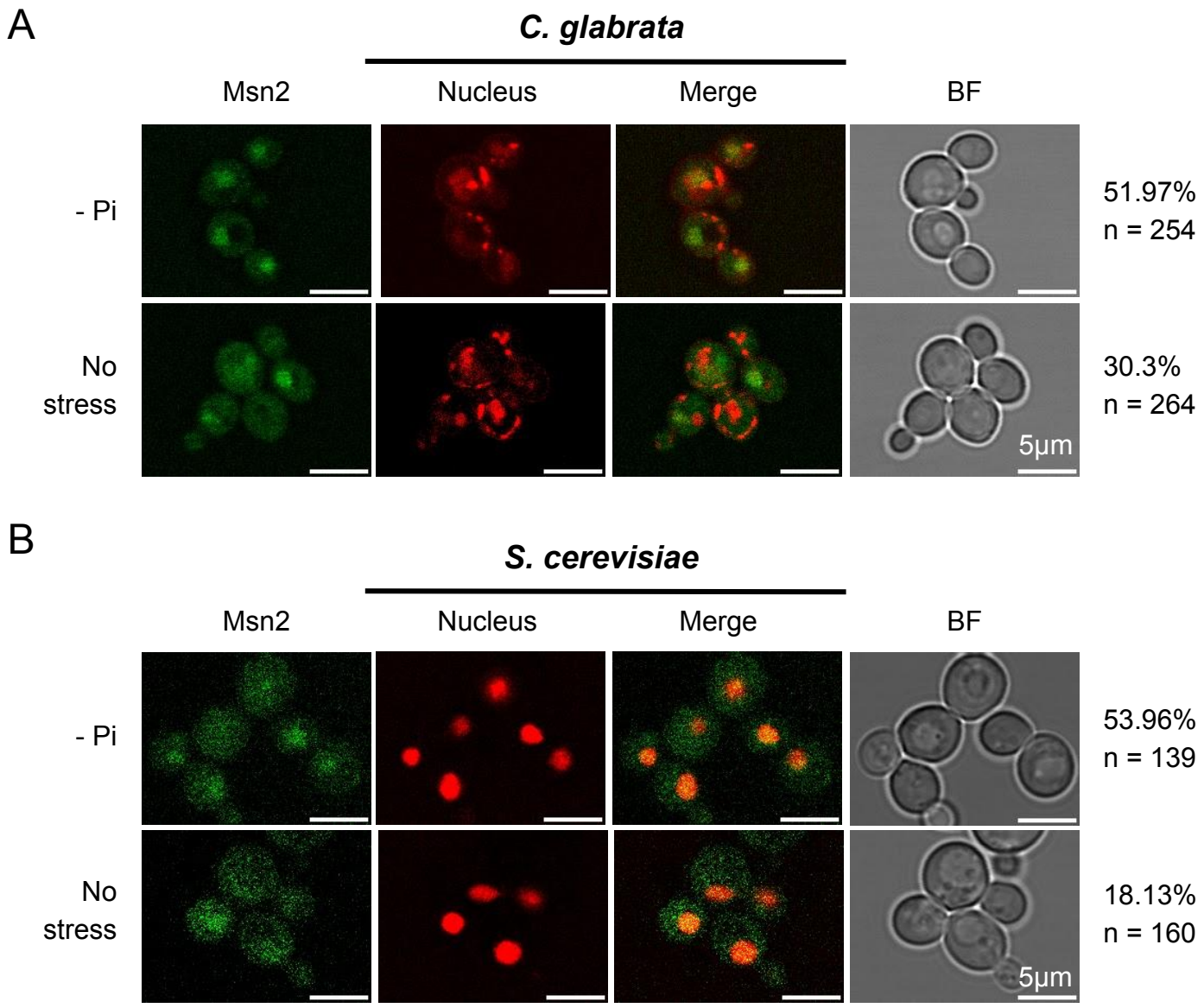

Supplementary Figure 8. *C. glabrata* Msn2 (CgMsn2) and *S. cerevisiae* Msn2 (ScMsn2) translocate into the nucleus upon phosphate starvation. Cellular localization of CgMsn2 (A) and ScMsn2 (B) under phosphate starvation (-Pi) and no stress conditions. All treatments were for 45 minutes. From left to right: i. CgMsn2-yeGFP and ScMsn2-mCherry (pseudo color); ii. nucleus staining with DAPI in *C. glabrata* or Nh6a-iRFP in *S. cerevisiae*; iii. merge of i and ii; iv. bright field; v. percentage of cells with nuclear-localized CgMsn2 or ScMsn2 under each condition (n=number of cells quantified). Scale bars all represent 5 µm in length. DAPI stain more than the nucleus in live *C. glabrata* cells as observed by others (Roetzer *et al.* 2008).

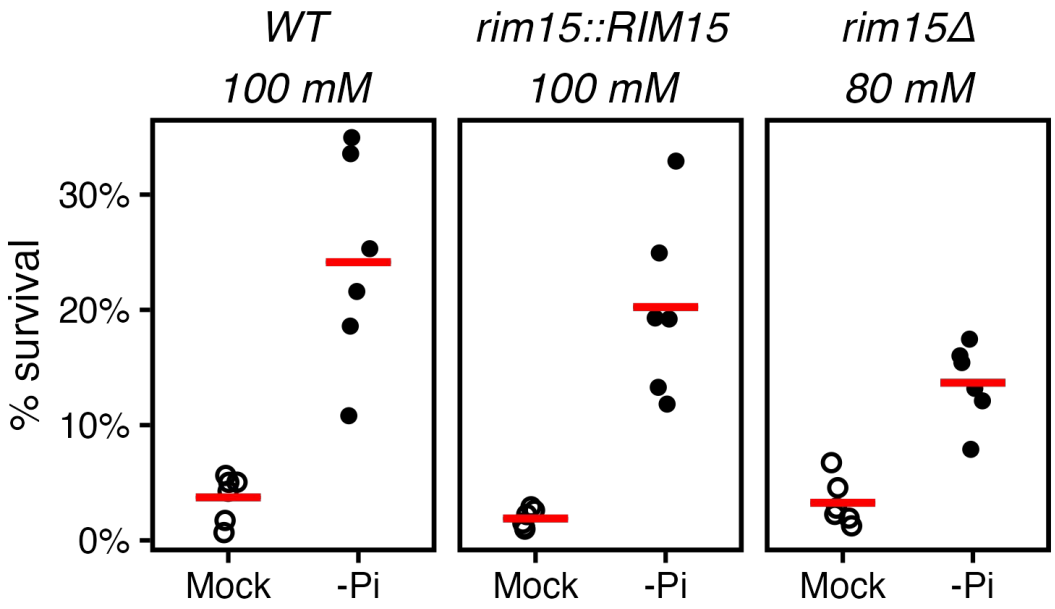

Supplementary Figure 9. *RIM15* complement strain rescues *rim15*Δ ASR defects. We restored *RIM15* at the endogenous locus on the *rim15*Δ background and compared its ASR effect to that in the wild type and *rim15*Δ strains. Concentrations of H_2O_2 were calibrated to achieve a similar basal survival rates (open circles, Kruskal-Wallis rank sum test among the three groups P = 0.27). ASR-scores for the three strains are (95% CI and Wilcoxon signed-rank test P-values in the parenthesis): wild type 9.5 ([5.3, 16.9], P=0.048); *rim15::RIM15* 11.6 ([8.6, 15.2], P=0.048); *rim15*Δ 5.3 ([3.4, 7.5], P=0.048). Based on Mann-Whitney U test, the ASR-score is not significantly different between either *rim15*Δ and wild type, or *rim15::RIM15* and wild type (Holm-Bonferroni-corrected P-values = 0.6 and 0.3, respectively). *rim15*Δ has relatively weak effects on ASR (Fig. 6D) and the wild type's survival rates with primary stress has relatively large variance in this experiment. Both could result in the lack of statistical significance in the comparison between *rim15*Δ and wild type. Instead, the difference in ASR-score between *rim15*Δ and *rim15::RIM15* has a P-value of 0.045. Combined, we conclude that *rim15*Δ reduces ASR and the complement strain rescues the defect.

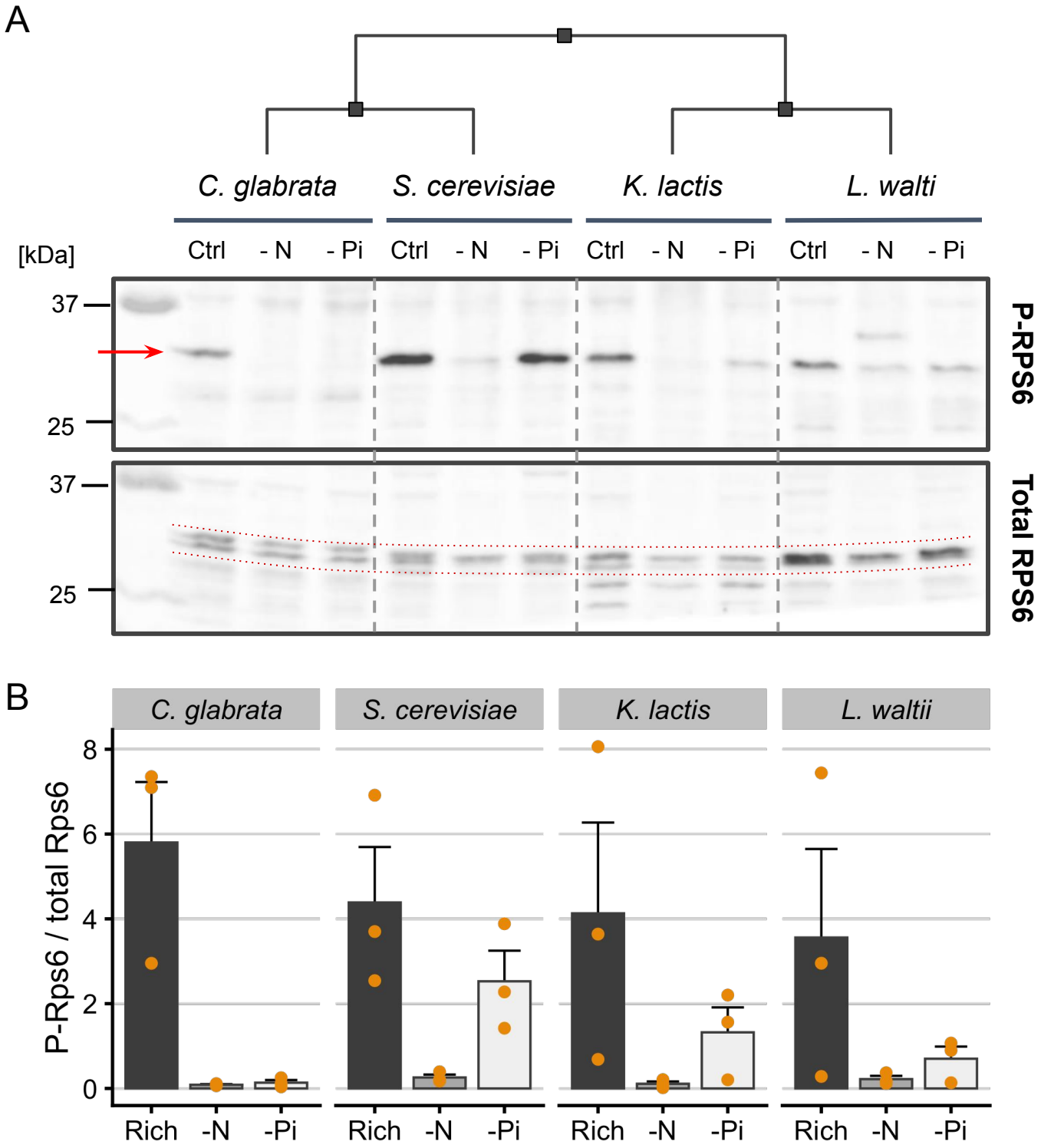

Supplementary Figure 10. TORC1 inhibition by phosphate and nitrogen starvation in diverse yeasts. (A) Western blot for P-Rps6 (top) and total Rps6 (bottom) in log phase *C. glabrata, S. cerevisiae, K. lactis* and *L. walti* cells, grown in rich, nitrogen starvation (-N) and phosphate starvation (-Pi) media for 1 hr at 30 ° C. This blot is representative of three biological replicates. The subset of the image including *S. cerevisiae* and *C. glabrata* was already shown in Fig. 7A. The cladogram on the top depicts the phylogeny between the yeasts; the arrow on the top blot indicates the band for the P-Rps6; the two dotted lines in the bottom blot indicate the bands for total Rps6 used for quantitative analysis. (B) Quantification of the ratio of P-Rps6 to total Rps6 based on three replicates. While the trend was obvious, the small sample size (3) limited the power of a paired Student's t-test used to compare the starvation conditions to the rich condition in each species, which resulted in *P*-values that were not significant at a 0.05 level after Bonferroni correction.

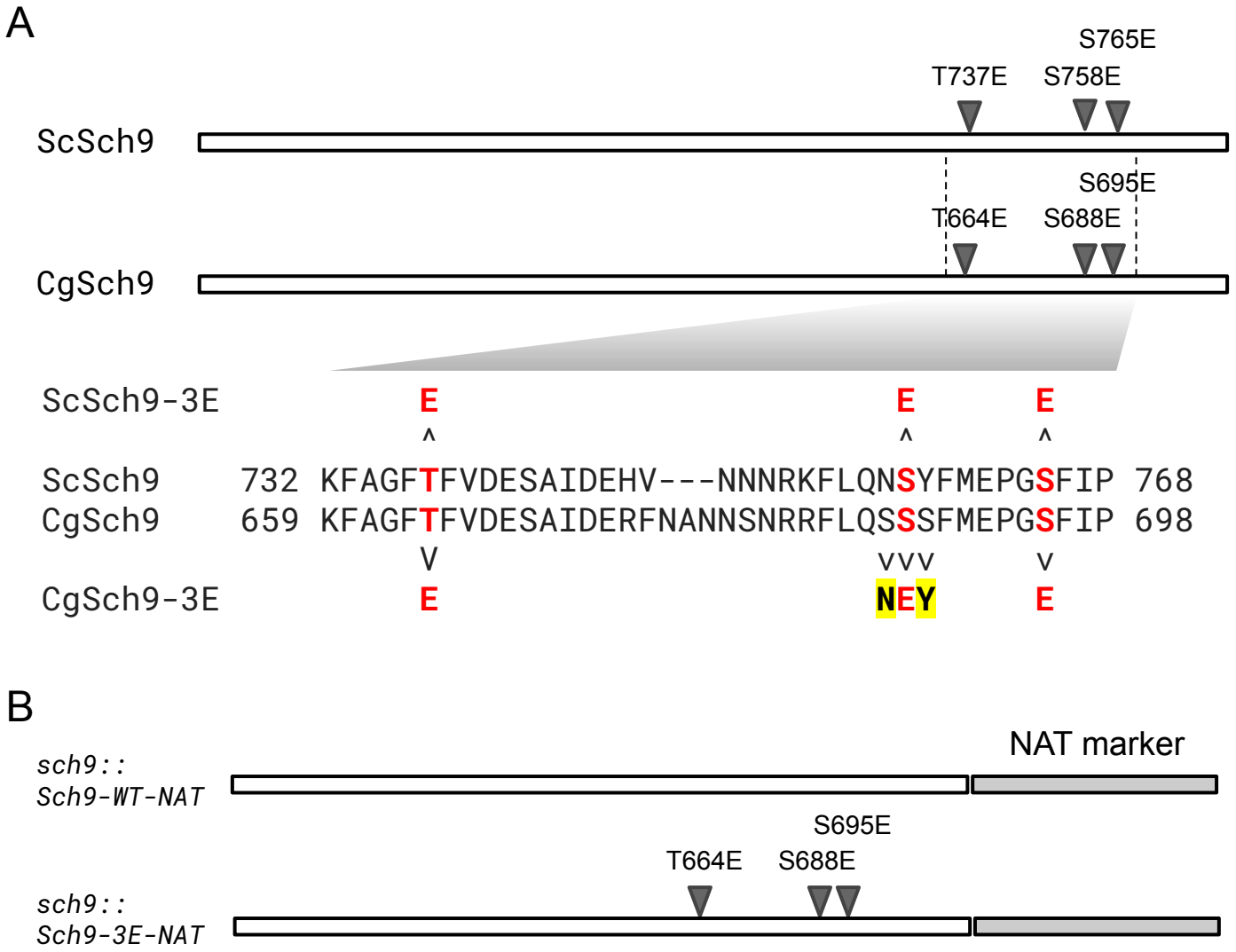

Supplementary Figure 11. Sch9-3E phosphomimetic mutant in *C. glabrata*. (A) Schematic alignment of Sch9 protein in *S. cerevisiae* and *C. glabrata*. The three TORC1 targeted S/T sites in ScSch9, based on Urban *et al.* 2007, and the corresponding sites in the orthologous CgSch9 based on the alignment were labeled with a triangle and the mutations were labeled on the top. The region containing the three S/T sites were shown below as a pairwise sequence alignment below. The S/T sites were shown in red bold fonts. For the second site, S758 (in ScSch9), the corresponding site in CgSch9 are flanked by two serines, making it difficult to determine whether and which serine may be the authentic phosphorylation site. We therefore decided to make three mutations to turn the site into the same sequence as in the ScSCH9-3E mutant. (B) To replace the endogenous *SCH9* gene in *C. glabrata* with the mutant alleles, we added an antibiotic NAT marker at the end of either the wild type *CgSCH9* gene or the *CgSCH9-3E* allele and performed allele swaps. The first construct provides a control for the effect of disrupting the 3' UTR by adding the NAT marker.

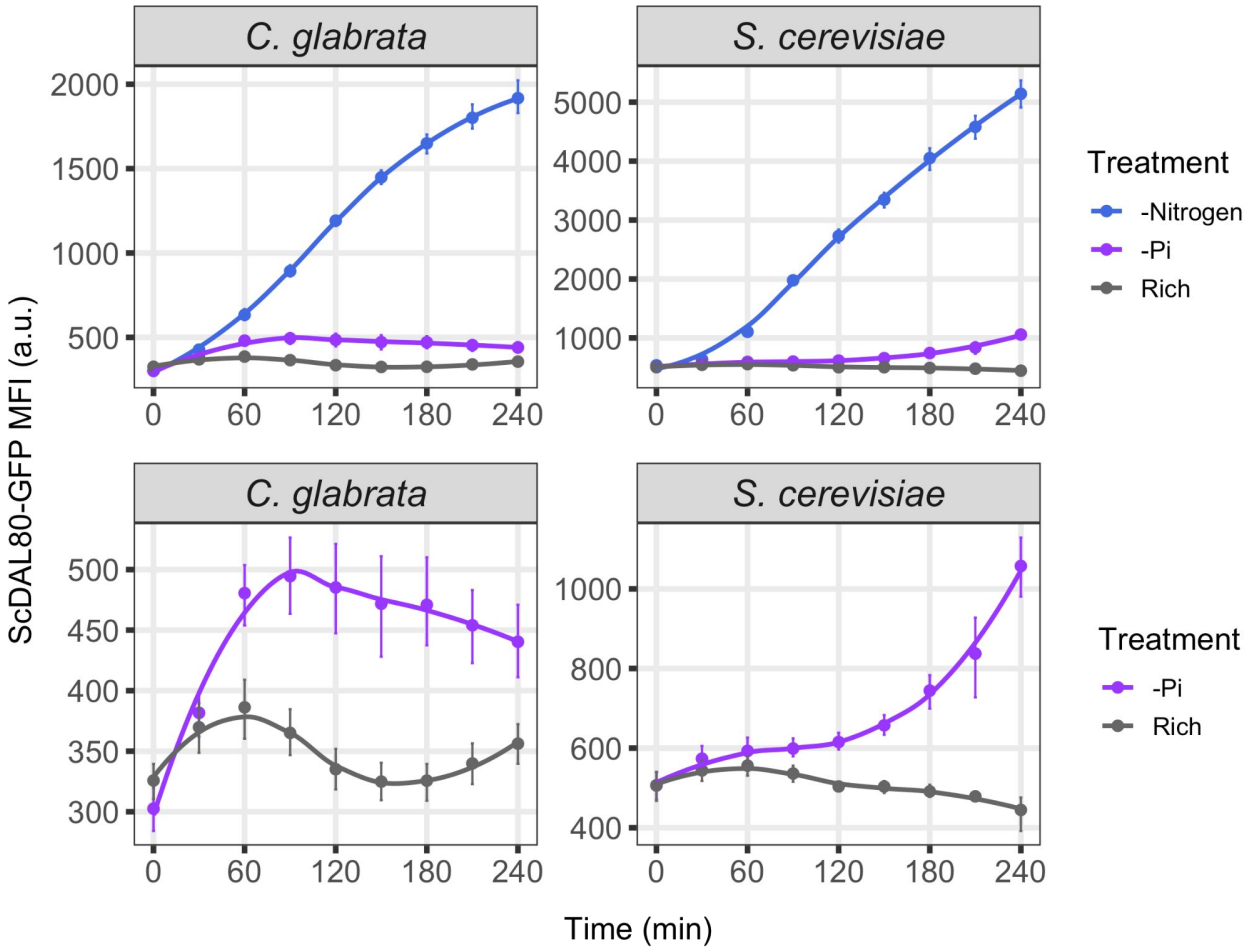

Supplementary Figure 12. *DAL80* induction kinetics under nitrogen and phosphate starvation in *S. cerevisiae* and *C. glabrata*. *ScDAL80pr*-GFP expression levels were monitored via flow cytometry over a time course of 4 hours during nitrogen (-N) or phosphate starvation (-Pi) and rich medium conditions. Dots represent the mean of Median Fluorescent Intensity from > 3 biological replicates; the error bars represent the 95% CI based on 1000 bootstraps. The lines are LOESS fit to the means. The top row shows all three conditions while the bottom row shows the same data without -N to better visualize the induction under -Pi.

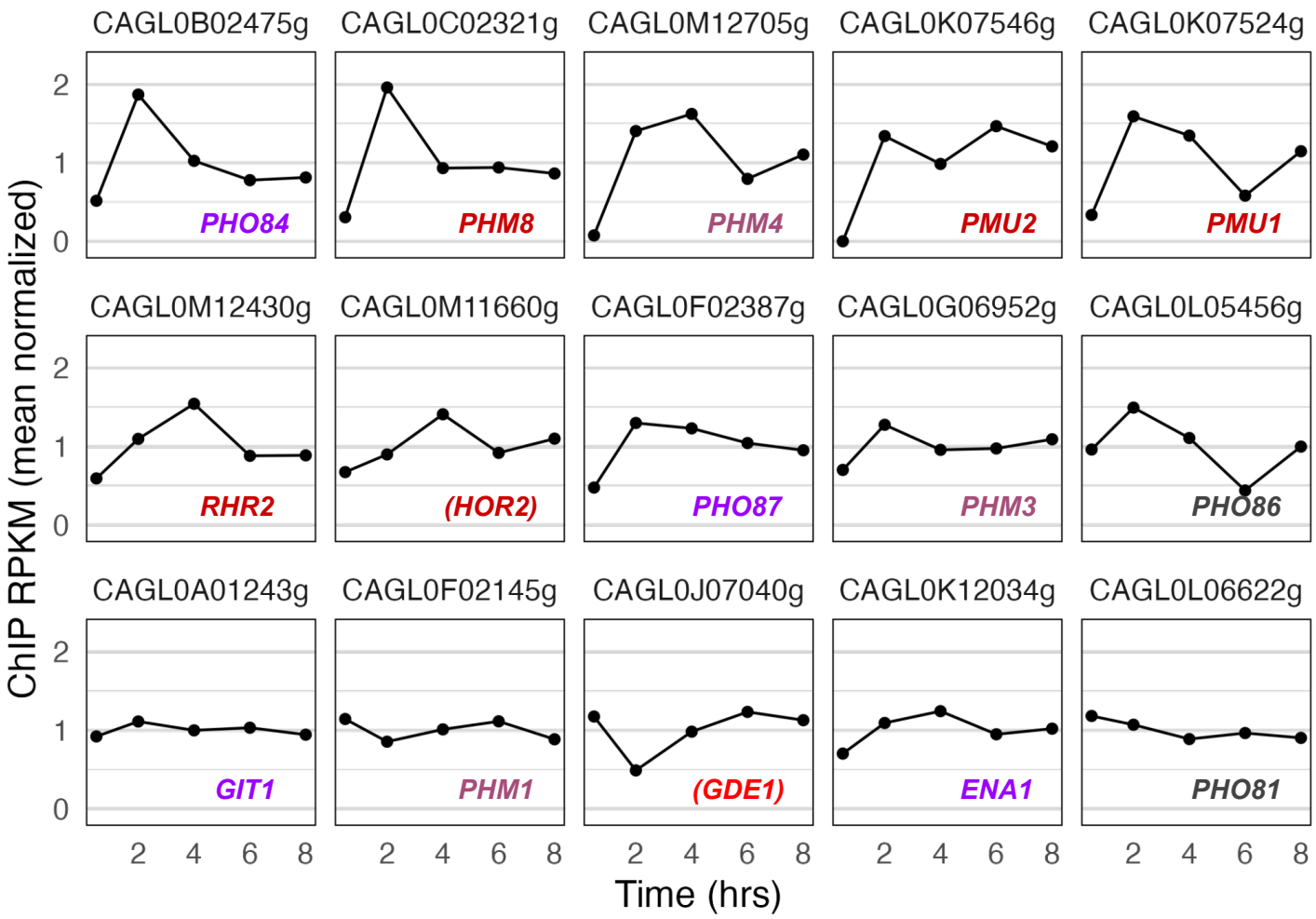

Phosphate transporters; Phosphatases; Phosphodiesterase; polyphosphate metabolism; regulatory

Supplementary Figure 13. Phosphate starvation response is partially induced in *C. glabrata* after the yeast is engulfed by human macrophages. Shown are the phosphate homeostasis genes induced during phosphate starvation in *C. glabrata*. Gene list is from (He *et al.* 2017). PolII ChIP-seq time course data are from (Rai *et al.* 2021), sampled at 0.5h, 2h, 4h, 6h and 8h post infection. For each gene, the ChIP-seq RPKM values were divided by the mean such that the normalized values represent fold changes over the mean for that gene. Systematic gene IDs were labeled on the top of each panel. Gene names were shown inside the panel (names in parentheses were based on *S. cerevisiae* homologs). Colors represented gene functional categories as explained below.

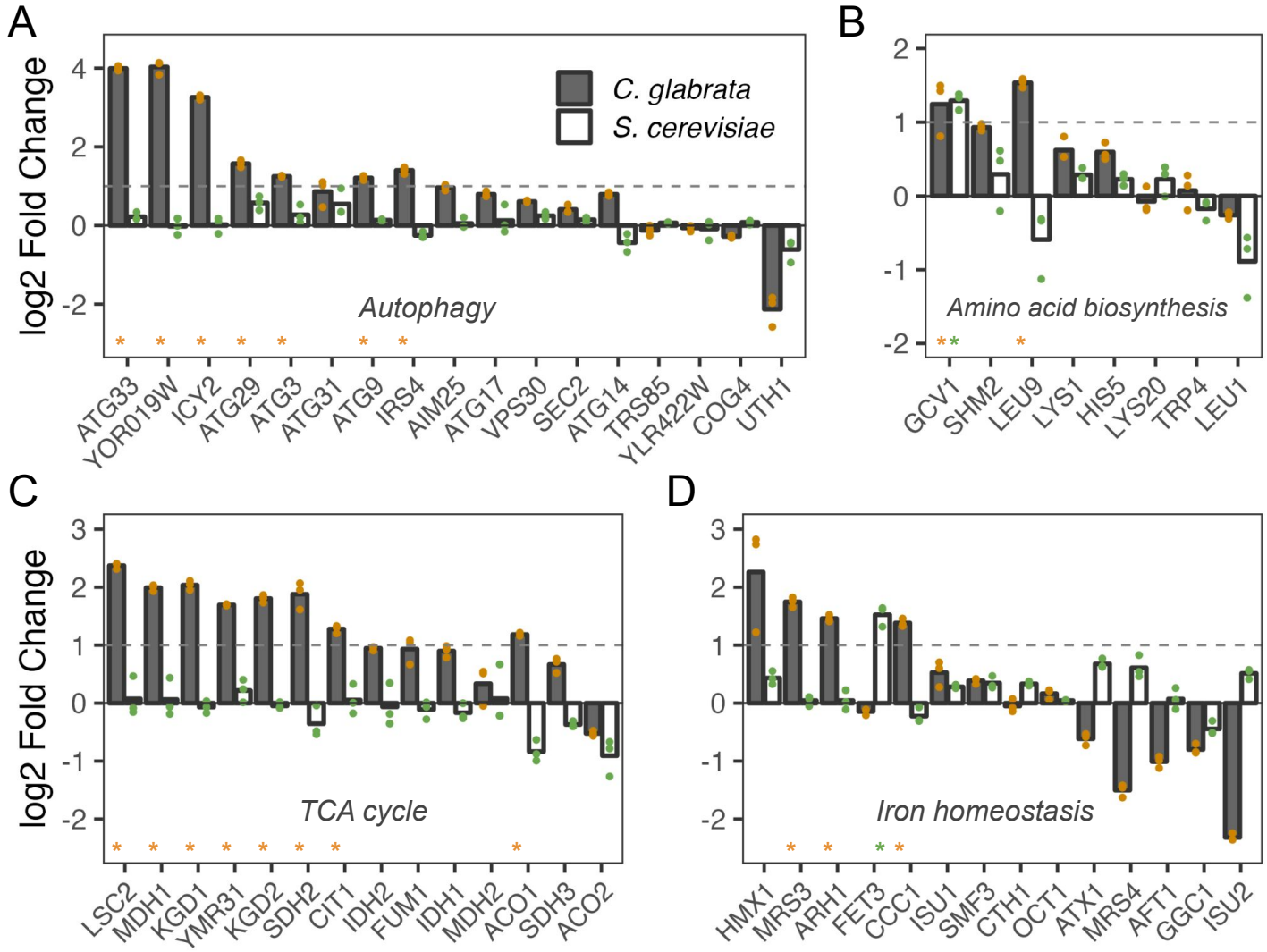

Supplementary figure 14. Genes induced after being engulfed by macrophages are also induced by a short-term phosphate starvation in *C. glabrata*. Data and plots are similar to Figure 2C-F. Gene sets were based on (Rai *et al.* 2021) supplementary figures 2 and 3 for figure 1. Gene names were based on *S. cerevisiae*. An asterisk meant the gene was significantly induced in the species at an FDR of 0.05.

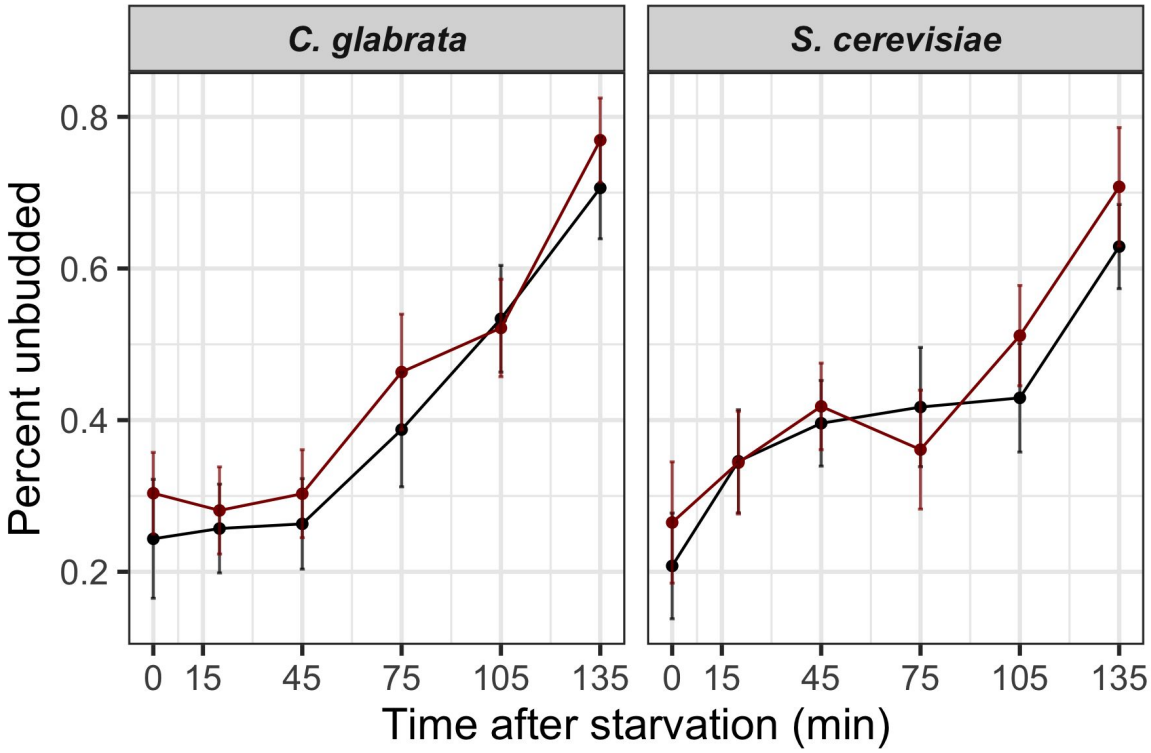

Supplementary Figure 15. Percent unbudded cells during phosphate starvation time course. Cells were taken at 0, 20, 45, 75, 105 and 135 minutes during the time course and assayed for cell morphology by light microscopy (Materials and Methods). The black and dark red dots and lines represent two biological replicates. The dots are the percentage of unbudded cells from >100 total cells examined. The error bars are the 95% confidence interval for the binomial proportion based on normal approximation (Wald Interval).